

GEOSPHERE, v. 15, no. 2

<https://doi.org/10.1130/GES01675.1>

14 figures; 6 tables; 1 animation; 1 set of supplemental files

CORRESPONDENCE: sgaynor@email.unc.edu

CITATION: Gaynor, S.P., Rosera, J.M., and Coleman, D.S., 2019, Intrusive history of the Oligocene Questa porphyry molybdenum deposit, New Mexico: Geosphere, v. 15, no. 2, p. 548–575, <https://doi.org/10.1130/GES01675.1>.Science Editor: Raymond M. Russo  
Associate Editor: Eric H. ChristiansenReceived 30 January 2018  
Revision received 12 October 2018  
Accepted 3 January 2019

Published online 5 March 2019



This paper is published under the terms of the CC-BY-NC license.

© 2019 The Authors

# Intrusive history of the Oligocene Questa porphyry molybdenum deposit, New Mexico

Sean P. Gaynor, Joshua M. Rosera\*, and Drew S. Coleman

Department of Geological Sciences, University of North Carolina at Chapel Hill, Chapel Hill, North Carolina 27510, USA

## ABSTRACT

Subsurface mapping and core analyses of upper crustal intrusions and mineralization at the Questa porphyry molybdenum deposit, New Mexico, reveal that Mo-mineralization occurred through episodic emplacement of at least six intrusive units. The structure of intrusions associated with the Questa deposit is documented in a series of detailed cross sections and visualized with a 3D animation. Mineralizing intrusions are underlain by two post-mineralization intrusions and cut by late-stage barren dikes. The plutonic complex was structurally focused along a system of preexisting flat-lying faults and their associated fractures. Mineralization is spatially associated with specific intrusive units in the subsurface, and the highest Mo ore grades within established ore blocks are structurally associated with the smallest intrusions. Existing U/Pb thermal ionization mass spectrometry (TIMS) zircon geochronology in conjunction with new relative chronology presented herein indicate that mineralization began before 24.91 Ma. We present three new chemical abrasion U/Pb TIMS zircon ages—one from an amphibole-bearing intrusion associated with high-grade mineralization (dark-matrix porphyry,  $24.74 \pm 0.37$  Ma), a rhyolite dike that cuts ore-grade rocks ( $24.50 \pm 0.02$  Ma), and an equigranular granite discovered during deep drilling ( $23.67 \pm 0.02$  Ma). The dark-matrix porphyry contains clasts of an earlier amphibole-free intrusion that is spatially associated with low-grade mineralization. Thus, mineralizing intrusions were, in part, intruded into slightly older porphyries, confirming that episodic mineralization continued after 24.91 Ma. The age of the barren dike ( $24.50 \pm 0.02$  Ma) is indistinguishable from that of a previously dated granite porphyry that is associated with low-grade mineralization (<0.05 wt% MoS<sub>2</sub>; Questa granite porphyry). These data suggest that mineralization waned by 24.5 Ma and that ore deposition occurred over ~500 ka. The new 23.67 Ma age of the deep equigranular granite, which underlies the Questa granite porphyry, further suggests that intrusions underlying the deposit were not related to mineralization. Detailed subsurface mapping and exploratory drilling indicate that intrusions associated with mineralization were small in volume and cooled rapidly, as evidenced by multiple internal contacts within sheets and rebcciation textures. On the basis of observed cross-section reconstructions, petrology, alteration, and mineralization, the porphyritic rhyolite intrusions associated with mineralization in one of the largest orebodies in the deposit (the deep northeast) are less than 20-m-thick sheets that are separated by andesite wall rock. Thus, there is no evidence that this orebody formed

\*Formerly Chevron Mining Inc., Questa, New Mexico 87556, USA

above a cylindrical magma conduit that facilitated rapid convection, as is often modeled in these systems. We hypothesize that a set of similarly small-volume intrusions were responsible for the bulk of the ore in the southwest ore zone. Our interpretation that the mineralizing intrusions are small, thin, and subhorizontal distinguishes the Questa deposit from other Climax-type molybdenum deposits.

## INTRODUCTION

Climax-type molybdenum (Mo) deposits are broadly described as hydrothermal-magmatic molybdenite mineralization associated with subvolcanic felsic intrusions. These deposits are characterized by high Mo concentrations (>0.10 wt% MoS<sub>2</sub>), reflecting a 400–1500x enrichment above upper-crustal average concentrations (1.5 ppm Mo) and even greater enrichment above lower-crustal concentrations (1.1 ppm Mo; Carten et al., 1993; Taylor and McLennan, 1995; Rudnick and Gao, 2003; Ludington and Plumlee, 2009). Magmas generating Climax-type deposits are also enriched in F, Rb, and Nb (Carten et al., 1993; Ludington and Plumlee, 2009). Mineralizing intrusions in Climax-type Mo intrusions are not auto-mineralizing; structural relationships and assay data suggest mineralizing fluids are mainly expelled outward from the crystallizing intrusions in the upper crust (Stein and Hannah, 1985; Carten et al., 1988; Shinohara et al., 1995). Molybdenite precipitates out of these hydrothermal fluids at a high temperature, proximal to its source intrusions (e.g., Mutschler et al., 1981; Carten et al., 1988; Burnham, 1997; Seedorff and Einaudi, 2004), resulting in a mineralized halo that partially overlaps the intrusive contact but lies mostly within the wall rock.

Climax-type deposits are commonly assembled following the volcanic peak within long-lived magmatic centers (e.g., Carten et al., 1993; Mercer et al., 2015a). They are typically interpreted to have been assembled as multiple discrete, relatively small-volume, cylinder-shaped intrusions (e.g., Wallace et al., 1968, 1968; White et al., 1981; Keith et al., 1986; Carten et al., 1988; Seedorff and Einaudi, 2004). These intrusions, and their associated hydrothermal cells, amalgamate to produce larger deposits and plutonic volumes (Carten et al., 1988). The complex amalgamation of intrusions and hydrothermal mineral assemblages results in a cyclical, or pseudo-cyclical, thermal history that is recorded in crosscutting alteration patterns (vein envelopes and pervasive alteration), changes in ore grade, and arrival of new magmas (Carten et al., 1988; Seedorff and Einaudi, 2004). Fluid-rich rock textures, such as crenulated unidirectional solidification textures—or “brain rock”—have been inferred to represent the accumulation of fluids near the apex of magma columns

(Shannon et al., 1982; Carten et al., 1988). These textures are subparallel to high-temperature alteration and high-grade mineralization in wall rocks and have been used to delineate contacts of texturally diverse, but mineralogically identical, mineralizing intrusions (Carten et al., 1988).

The Mo abundances observed in Climax-type deposits are commonly interpreted to be result of streaming volatiles and metals concentrated from a structurally deeper, low-(Mo), fractionating magmatic reservoir (e.g., Keith and Shanks, 1985; Lowenstern, 1994; Klemm et al., 2008; Seo, 2014; Audébat, 2015; Mercer et al., 2015a). In these models, a magmatic cupola serves as a conduit for lower-density fluids that combine with fluids exsolving from the crystallizing and convecting magma to form the hydrothermal system (Shinohara et al., 1995). Predicted rates of magma convection within these conduits are on the order of tens of km/a, which is orders of magnitude higher than the predicted rate at which large volumes of magma become unstable and eventually erupt from the upper crust (Annen, 2009). Although the final size of porphyry Mo deposits is much smaller than caldera-forming magma systems, the difference in estimated magma flux is dramatic.

More recent studies of porphyry Mo systems suggest that a persistent magma conduit may not be required for focusing fractionated fluids into the upper crust. Instead, they suggest that mineralization is accomplished through multiple discrete events during protracted assembly of intrusions (e.g., Chiariadis et al., 2014; Chelle-Michou et al., 2015; Mercer et al., 2015b). Thus, an alternate explanation is that the feeder conduits are short-lived features that act to pass magma and volatiles from deeper parts of the system; convection within the conduit might be an unnecessary component.

Recent exploratory drilling at the Questa Climax-type Mo deposit in northern New Mexico, USA, identified mineralizing intrusions with geometries that differ from the typical cylindrical magma bodies depicted in other studies (Figs. 1 and 2). The Questa deposit therefore provides an intriguing opportunity to investigate the role of cylindrical melt columns in the history of Mo deposition. Mineralization at the Questa deposit has been interpreted to be the result of two stages of hydrothermal fluid exsolution from a large, fractionating magma chamber (Klemm et al., 2008; Greber et al., 2014). In this study, core logs, assay data, field maps (surface and underground drift maps), and detailed deposit cross sections were compiled to generate a more complete understanding of the magmatic and mineralization history at Questa. New thermal ionization mass spectrometry (TIMS) U-Pb zircon geochronology provides a more complete understanding of the absolute timing of magmatism and mineralization. These data are combined to build a three-dimensional fence diagram, and a new model of the Questa Mo deposit which characterizes the volume, shape, relative metal contribution, and timing of each intrusion in the ore deposit.

## GEOLOGIC SETTING

The Questa Mo porphyry deposit is located in the Latir volcanic field of north-central New Mexico (Figs. 1 and 2). The region hosted economic and

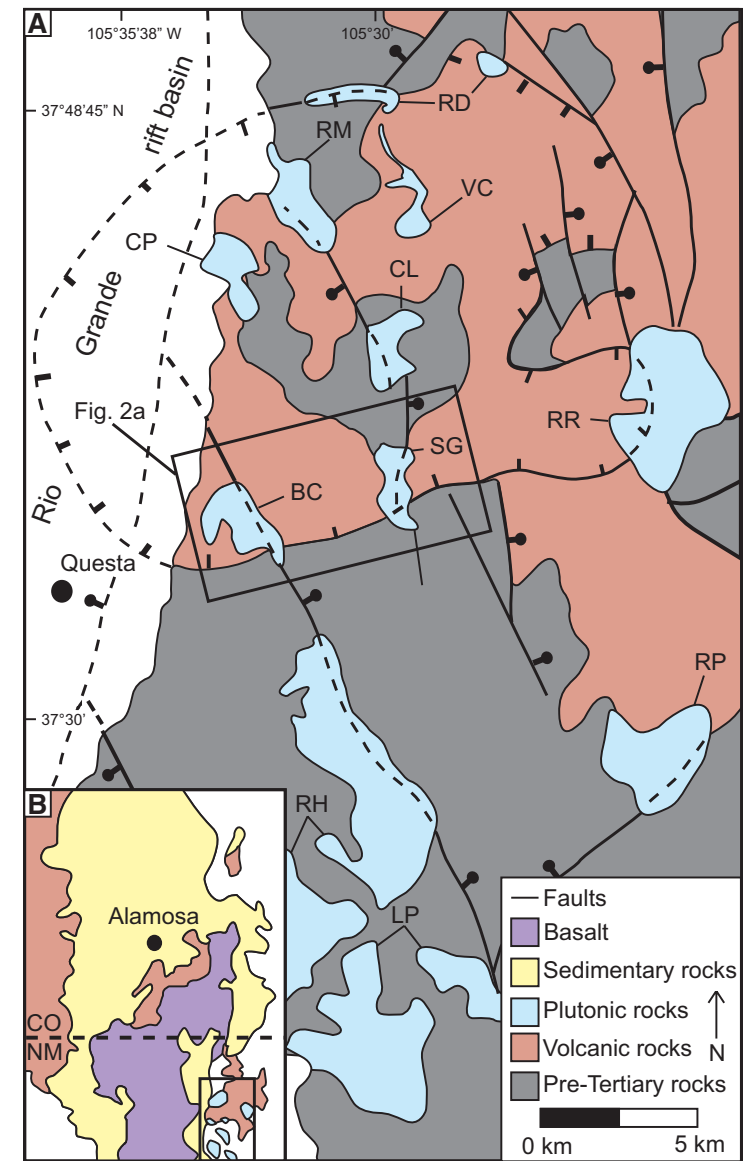


**Figure 1.** Generalized geologic map of (A) the Latir magmatic field and Questa caldera showing the distribution of the volcanic and plutonic rocks (after Lipman and Reed, 1989) and (B) the northern Rio Grande rift. Abbreviations for the plutonic units are (from oldest to youngest): RD—ring dike; VC—Virgin Canyon; RM—Rito del Medio; CP—Cañada Pinabete; CL—Cabresto Lake; BC—Bear Canyon; SG—Sulphur Gulch; RR—Red River intrusive suite; RH—Rio Hondo; RP—Relica Peak; LP—Lucero Peak. Location of Figure 1A is indicated by the box in Figure 1B. CO—Colorado; NM—New Mexico.

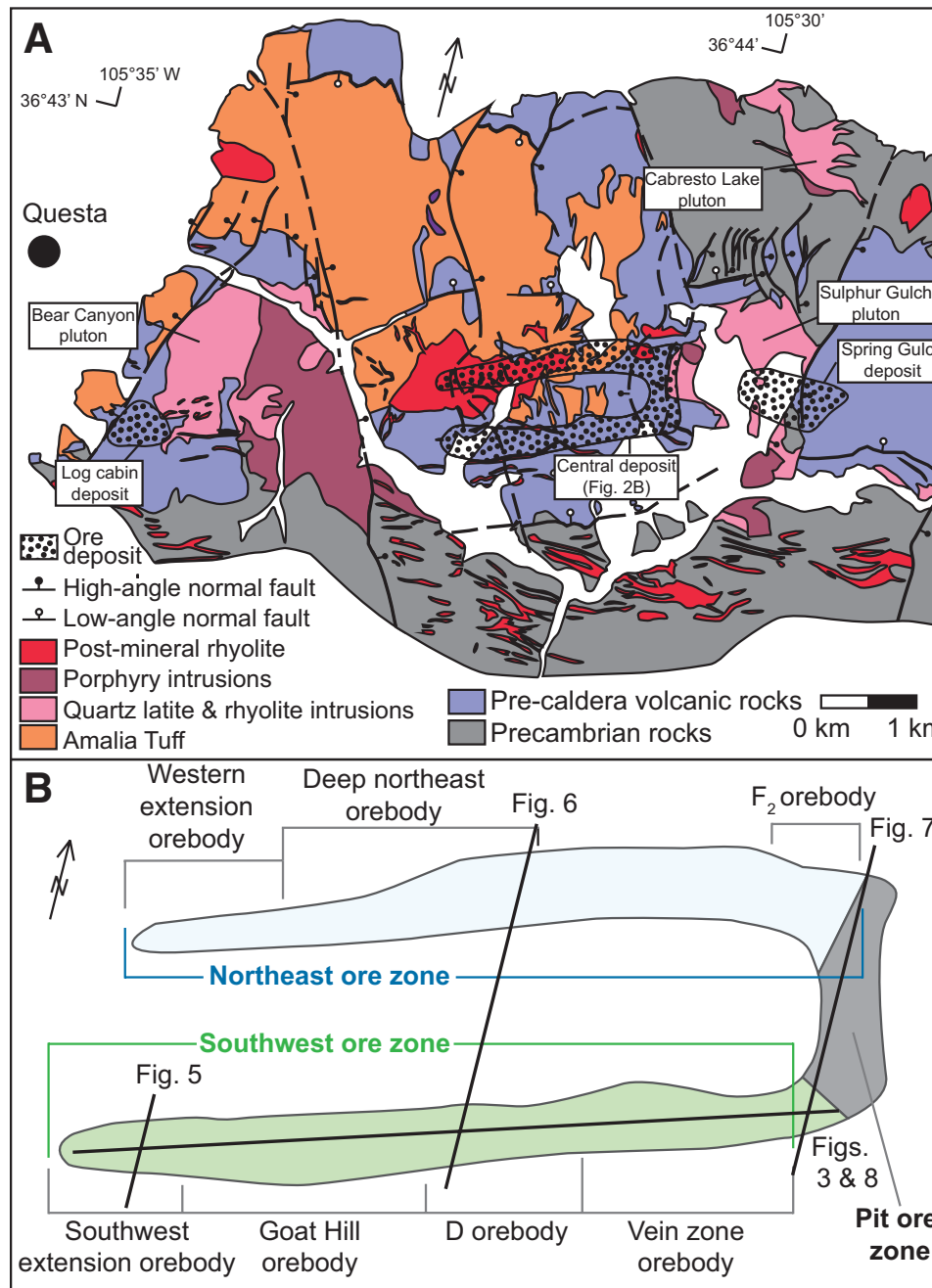


Figure 2. (A) Map showing the generalized surficial geology in the vicinity of the Questa ore deposits (note that north is rotated 14° clockwise). Ore deposits approximately correspond to 0.2 wt% MoS<sub>2</sub> contours projected to the surface. Map data from Meyer (1991). (B) Hierarchy and nomenclature in the central deposit at the Questa porphyry Mo deposit. Note that three ore zones each comprise multiple orebodies. See text for discussion.

noneconomic magmatism during a 10 Ma magmatic history between 29 and 19 Ma (Table 1; Lipman et al., 1986; Tappa et al., 2011; Zimmerer and McIntosh, 2012; Rosera et al., 2013). Cenozoic volcanism within the Latir field ranges from andesite to rhyolite, with several tuffs erupted prior to peak magmatism that is marked by the eruption of the ~500 km<sup>3</sup> Amalia Tuff at 25.5 Ma and formation of the Questa caldera (Tappa et al., 2011; Zimmerer and McIntosh, 2012). Exposed plutonic rocks intruded following the eruption of the Amalia tuff and span at least 6 Ma of magmatic history from 25.3 to 19.1 Ma (Tappa et al., 2011; Zimmerer and McIntosh, 2012; Rosera et al., 2013). Postcaldera magmatism is primarily preserved as resurgent and shallow intrusions that become younger and structurally deeper to the south (Lipman et al., 1986). Caldera margin plutons (Bear Canyon pluton, Sulphur Gulch pluton, and Red River intrusive complex; Fig. 1) are intermediate in age among exposed plutonic rocks and have the closest spatial associations with economic mineralization at Questa (Meyer and Foland, 1991; Zimmerer and McIntosh, 2012; Rosera et al., 2013). Porphyry Mo mineralization at the Questa deposit within the caldera margin began ca. 24.9 Ma and continued episodically until at least 24.5 Ma, with multiple discrete mineralization events identified through geochronology (Rosera et al., 2013). Fluid inclusion studies indicate that mineralizing intrusions intruded between 3 and 5 km depth (Cline and Bodnar, 1994). Younger plutons (ca. 23.5–22.5 Ma) are unmineralized (Tappa et al., 2011).

Rio Grande rift extension began regionally at ca. 28 Ma, coeval with the onset of magmatism within the Latir (Olsen et al., 1987; Zimmerer and McIntosh, 2012; Ricketts et al., 2016). The caldera was extended up to 200% by early rifting and developed a system of low-angle normal faults that facilitated the rotation of the welded Amalia tuff and intercalated andesite megabreccia fragments to near vertical orientations along the southern caldera margin (Meyer and Foland, 1991; Fig. 2). One of the low-angle normal faults is cut by a  $24.91 \pm 0.07$  Ma porphyritic intrusion ~1 km southeast of the Questa pit mine (Meyer and Foland, 1991; Rosera et al., 2013), thereby limiting the timing of rotation to have been between the eruption of the Amalia tuff at 25.52 Ma and 24.9 Ma (Tappa et al., 2011). Paleomagnetic studies also indicate that plutons along the southern caldera margin did not experience significant

tilting (Snyder, 1984; Hagstrum and Johnson, 1986; Hagstrum and Lipman, 1986). Numerous brittle fault zones were identified above some orebodies and porphyritic intrusions in the subsurface of the Questa Mo mine (Ross et al., 2002). The gentle northerly dips of low-angle faults (~10°–20°) was interpreted to be a preexisting anisotropy that helped facilitate pluton assembly and formation of flat-lying magmatic-hydrothermal breccia bodies (within the Questa Mo deposit), which also gently dip to the north (Meyer, 1991; Ross et al., 2002). Extension postdating intrusive activity within the Latir is exposed as deeply penetrating, high-angle normal faults that are parallel to subparallel to range-bounding faults (Hagstrum and Lipman, 1986; Meyer and Foland, 1991). Minor block tilting of the Latir continued as recently as 15 Ma (Lipman, 1983).

## Geology of the Questa Ore Zone

The Questa ore zone is divided into three major deposits: from east-to-west, these are the Spring Gulch deposit, the central deposit, and the log cabin deposit (Fig. 2A). On the basis of drill-core data and subsurface mapping, the Spring Gulch deposit is thought to be associated with the Sulphur Gulch pluton, and the log cabin deposit is considered to be associated with the Bear Canyon pluton. The central deposit is associated with both the western part of the Sulphur Gulch pluton and the southwest intrusive suite—an unexposed and previously undifferentiated unit of rhyolite and granite porphyries (Fig. 3; Ross et al., 2002; Rosera et al., 2013). The central deposit was the target of all historic Mo mining within the Questa ore zone and includes discrete orebodies as defined by the historical economic cutoff of 0.2% MoS<sub>2</sub> (Fig. 2; Ross et al., 2002; McLemore and Mullen, 2004).

The central deposit (the focus of this study) includes three ore zones: the northeast ore zone, the southwest ore zone, and the pit ore zone (Fig. 2B). Total MoS<sub>2</sub> mineralization in the deposit is estimated to be 398,880 tons (Ludington and Plumlee, 2009). Historically, open pit and underground mining were done in the pit ore zone, but more recent underground mining was located in the southwest ore zone. Orebodies within the southwest ore zone are broken into

TABLE 1. RELATIVE AND ABSOLUTE CHRONOLOGY OF THE LATIR MAGMATIC CENTER

Geologic unit	Age (Ma)*	Reference
Rio Hondo <sup>t</sup>	$22.98 \pm 0.09$ ; $22.84 \pm 0.06$ ; $22.72 \pm 0.05$ ; $22.59 \pm 0.06$	Tappa et al. (2011)
Southwest Intrusive Suite	$24.53 \pm 0.045$ ; $24.46 \pm 0.05$ ; $24.44 \pm 0.086$	Rosera et al. (2013)
Sulphur Gulch Pluton	$24.91 \pm 0.069$	Rosera et al. (2013)
Cabresto Lake Pluton	$25.09 \pm 0.04$ ; $25.02 \pm 0.05$	Tappa et al. (2011)
Red River Intrusive Suite	$25.21 \pm 0.055$ ; $25.20 \pm 0.036$	Rosera et al. (2013)
Cañada Pinabete Pluton	$25.29 \pm 0.05$	Tappa et al. (2011)
Amalia Tuff	$25.52 \pm 0.06$	Tappa et al. (2011)
Pre-Amalia volcanic rocks	§Ca. 29–27	Zimmerer and McIntosh (2012)

\*All dates are chemical abrasion–thermal ionization mass spectrometry U/Pb zircon geochronology unless otherwise noted.

<sup>t</sup>The Rio Hondo is a downward-stacking pluton, with geochronologically defined phases.

§Ar-Ar geochronology, due to the lack of published zircon geochronology.

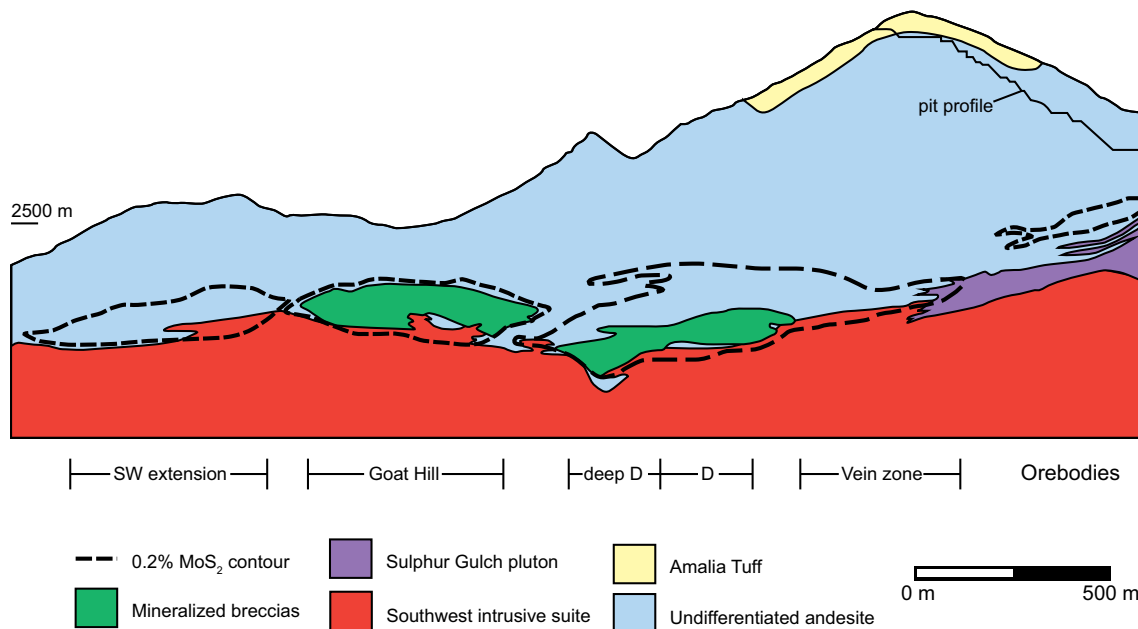


**Figure 3.** Cross section through the central deposit (see Fig. 2) modified from Ross et al. (2002). These authors did not differentiate units within the southwest intrusive suite. Studies of the magmatic-hydrothermal breccia bodies located at the roof of the suite noted meter-scale variations in isotopic composition and fluid inclusion homogenization temperature of hydrothermal assemblages (Ross et al., 2002; Rowe, 2012). Recent Re-Os molybdenite geochronology suggests the Goat Hill orebody was assembled during discrete events from ca. 24.8–24.5 Ma (Rosera et al., 2013). These studies all suggest that multiple hydrothermal events are associated with the formation of the breccia bodies and, therefore, the underlying southwest intrusive suite.

four orebodies: the vein zone orebody, the D-orebody, the Goat Hill orebody, and the southwest extension orebody. The northeast ore zone is broken into the F<sub>2</sub> orebody, the deep northeast orebody, and the western extension orebody (Fig. 2B).

Alteration and mineralization at the Questa deposit are the result of felsic porphyry intrusions that form a structurally complicated sequence of cross-cutting igneous bodies and altered hydrothermal breccias (Ross et al., 2002). Hydrothermal-magmatic alteration and vein thermometry are broadly grouped into four classes of alteration (Table 2; Bloom, 1981; Cline and Bodnar, 1994; Ross et al., 2002; Klemm et al., 2008; Rowe, 2012). These alteration assemblages and their paragenesis are typical of other porphyry systems (e.g., Lowell and Guilbert, 1970; Seedorff and Einaudi, 2004) in that the ore zone is characterized by high-temperature (375–550 °C) mineral assemblages with abundant quartz, K-feldspar, and molybdenite in veins and vein envelopes. Biotite that formed via potassio alteration within the volcanic wall rock (Ross et al., 2002) is also common at Questa. Large volumes of rock are overprinted by moderate-temperature sericitic ( $\pm$ quartz  $\pm$  pyrite  $\pm$  magnetite) alteration assemblages. Low-temperature alteration typically includes clay alteration of feldspars + pyrite  $\pm$  calcite. As for other Climax-type systems, late-stage fluorite, galena, sphalerite, and rhodochrosite are also common expressions of low-temperature alteration (Seedorff and Einaudi, 2004). Economic Mo mineralization is associated with high-temperature silicic alteration, estimated to have occurred

between 380° to 550 °C on the basis of fluid inclusion data (Fig. 4; Table 2; Cline and Bodnar, 1994; Klemm et al., 2008; Rowe, 2012).

The occurrence of molybdenite at Questa can be categorized into three types. The majority of molybdenite is hosted in stockwork veins that are typically less than a few millimeters in thickness. Clotty molybdenite occurs within the matrix of magmatic-hydrothermal breccia bodies that are associated with the roofs of felsic intrusions (MHBX, Fig. 4; Ross et al., 2002). Disseminated molybdenite is volumetrically minor and localized within the deposit. Numerous examples of stockwork veins cutting hydrothermal breccia are documented (Ross et al., 2002; Klemm et al., 2008); however, recent geochronology indicates that multiple discrete episodes of brecciation and vein formation during the formation of the MHBX cannot be characterized by a singular progression from breccia stage to vein stage (Rosera et al., 2013).

The association of high-Mo grade with the hydrothermal breccia bodies, and the volume and proximity of the breccias above intrusions, led to the interpretation that the mineralization was the result of direct volatile exsolution from shallow intrusions (Ross et al., 2002). Within hydrothermal breccias, alteration is zoned from high-temperature potassio alteration near the lower contact with the inferred mineralizing intrusion to lower-temperature sericitic alteration near the roof of the breccia. However, fluid inclusion homogenization temperatures are not spatially as simple as the alteration zones, and Re-Os geochronology of molybdenite samples reveals age variation beyond analytical uncertainty,

TABLE 2. ALTERATION FACIES AND THERMOMETRY  
OF THE QUESTA PORPHYRY MO DEPOSIT

Alteration style*	General mineralogy <sup>†</sup>	Temperature (°C) <sup>†</sup>
<b>High-temperature</b>		
Quartz-molybdenite	Quartz + molybdenite ± fluorite ± K-feldspar ± pyrite	375–550
<b>High- to moderate-temperature</b>		
Biotite-K-feldspar	Quartz + biotite + K-feldspar ± molybdenite ± phlogopite	325–500
Biotite	Quartz + biotite ± pyrite	
K-feldspar-quartz	K-feldspar + quartz ± molybdenite ± sericite	
K-feldspar-magnetite	K-feldspar + magnetite + quartz ± molybdenite ± pyrite	
<b>Moderate-temperature</b>		
Sericite-magnetite	Quartz + magnetite ± biotite ± pyrite ± sericite	250–400
Sericite-pyrite	Quartz + sericite ± pyrite ± calcite ± molybdenite	
<b>Low-temperature</b>		
Pyrite-clay-carbonate	Pyrite ± clay ± calcite	
Calcite-fluorite	Calcite ± fluorite ± pyrite ± quartz	
Base metals	Galena ± sphalerite ± cassiterite ± quartz ± calcite ± pyrite	75–220
Rhodochrosite	Rhodochrosite ± fluorite ± calcite	

\*Alteration styles adapted from Seedorff and Einaudi (2004).

<sup>†</sup>Alteration facies and thermometry data compiled from Bloom (1981), Cline and Bodnar (1994), Ross et al. (2002), Klemm et al. (2008), Rowe (2012), and Seo (2014).

suggesting that alteration of the breccias did not result from single cooling events (Rowe, 2012; Rosera et al., 2013). This agrees with geochronology and geochemistry from other porphyry deposits, where mineralization is the result of multiple discrete events (e.g., Chiaradia et al., 2014; Chelle-Michou et al., 2015; Mercer et al., 2015b).

## METHODS

### Mapping

Underground drift maps from ~160 km of workings and drill-core logs from ~270 km of exploration wells were compiled and analyzed on the basis of crosscutting relationships, unit descriptions, and alteration. Where available, core photos, previously logged core, and legacy core logs were used to evaluate earlier observations. All previous interpretations of the geology relating to Mo mineralization (Martineau et al., 1977; Lipman and Reed, 1989; Meyer, 1991; Ross et al., 2002; Hoag, 2004) were organized to permit comparison with new observations. Delineation of rock units by review of drill-core and subsurface map data was limited by incomplete or inconsistent core logs and photos for older cores. Moreover, lithological contacts were often ignored or

not recognized in old logs that only identified named rock types with no rock descriptions. Consequently, we constructed a new database of intrusive features including unidirectional solidification textures (e.g., “brain-rock” textures and crenulate quartz veining; Shannon et al., 1982; Carten et al., 1988) and mosaic (intrusive-contact) breccias (Ross et al., 2002; Fig. 4). Brain-rock textures are composed of crenulated layers of often euhedral quartz and K-feldspar that typically range from 1–20 mm thick (Fig. 4A). Quartz crystals terminate in the direction of their parental liquid and are interpreted to grow away from solid substrates (Shannon et al., 1982). Similar textures have been described at the Henderson Mo mine where they are observed in the border phases of temporally discrete intrusions. We paid particularly close attention to brain-rock textures to help delineate contacts between previously undifferentiated intrusions and generate a more complete set of intrusive rock contacts and units. In many cases, intrusive-contact features project from established contacts through older drill holes where contacts between multiple intrusions had been overlooked in previous studies.

The presence and density of alteration veins were also documented, with an emphasis on identifying hydrothermal temperature reversals (e.g., low-temperature veins cut by high-temperature alteration veins) indicative of thermal cycling within the hydrothermal system (e.g., Seedorff and Einaudi, 2004). Vein and roof contact orientations were collected and compiled throughout the subsurface of the Questa mine and plotted using Stereonet 9.5 (Allmendinger et al., 2011; Cardozo and Allmendinger, 2013).

A series of N-S geologic cross sections was made of the southwest ore zone in 61 m intervals, with several sections extending into the northeast ore zone where significant drill data are available. Using the interpretations made in these N-S geologic cross sections, and additional core data, a SW-NE cross section was generated across the southwest ore zone, parallel to strike of the orebodies. An E-W cross section of the deep northeast ore zone was constructed using the same methods. Fence diagram models were generated in SketchUp (2016). Cross sections and 3-dimensional reconstructions were used to estimate the orientations and volumes of intrusive units.

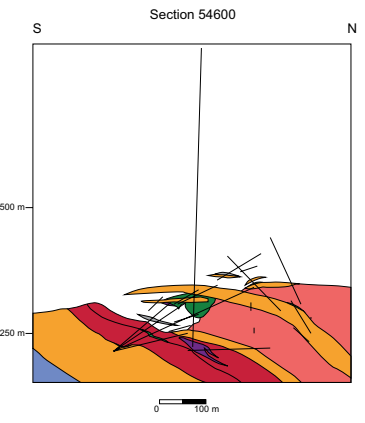
### Zircon Geochronology

Samples of a mineralized porphyritic latite (DD-9-651), a barren dike (DNE-5-3051), and the deep equigranular granite (DNE-1-3905) were dated using zircon U/Pb geochronology in order to better determine the timing and end of Mo mineralization at Questa. Sample DD-9-651 was collected from drill core from the deep D orebody, and samples DNE-1-3905 and DNE-5-4051 were collected from exploratory drilling of the deep northeast orebody (Fig. 2B).

Samples were prepared by crushing using a jaw crusher and a disc mill. Zircon was isolated using standard density (water table and heavy liquids) and magnetic separation techniques. Individual grains were selected using a binocular microscope to represent the range of size and morphology present in the samples. Selected zircon grains were thermally annealed for 48 h at



**Figure 4.** Representative alteration textures and crosscutting relationships from the central deposit: (A) Unidirectional solidification textures (UST), specifically brain rock, found at the roof of the main sheet of central aplite (DD-11-600). (B) Photo and annotated photo of the roof of a sheet of dark-matrix porphyry (DD-9-656). This contact has meter-scale breccia, hosting clasts of altered central aplite encased in altered dark-matrix porphyry. High-temperature alteration veins within clasts of the central aplite terminate at the margins of the clast, indicating high-temperature alteration of the central aplite predated emplacement and alteration of the dark-matrix porphyry. (C) Magmatic-hydrothermal breccia (MHBX) from the southwest extension orebody, located structurally above the central aplite (SWE-2 98.5–993.5). The breccia includes clasts of altered andesite wall rock (dark) encased by hydrothermal alteration veins (light). Gray faces within fractured quartz veins are vein molybdenite. This breccia shows multiple alteration events, identified by early generations of quartz veins offset by later veins. (D) Potassium feldspar-quartz-molybdenite veins cutting the central aplite in the southwest extension orebody, with potassium feldspar alteration envelopes surrounding veins (SWE-6 148).



<sup>1</sup>Supplemental Items. Contains 29 additional cross sections detailing the subsurface geology of the Oligocene Questa porphyry deposit. Please visit <https://doi.org/10.1130/GES01675.S1> or access the full-text article on www.gsapubs.org to view the Supplemental Items.

900 °C and then chemically abraded for 4–12 h at 220 °C in order to eliminate volumes affected by radiation damage and to remove inclusions (Mundil et al., 2004; Mattinson, 2005). All zircon analyses were made on single crystals. Zircons were spiked using a  $^{205}\text{Pb}$ - $^{233}\text{U}$ - $^{236}\text{U}$  tracer (Parrish and Krogh, 1987) and dissolved following a procedure modified after Krogh (1973) and Parrish (1987). Isolation of U and Pb was accomplished using HCl anion exchange chromatography procedures modified after Krogh (1973).

Isotope ratios of both U and Pb were determined using an IsotopX Phoenix-X62 (samples DD-9-651 and DNE-5-3051) or VG Sector 54 (sample DNE-1-3905) thermal ionization mass spectrometer (TIMS) at the University of North Carolina at Chapel Hill. Uranium was run as an oxide after loading in silica gel on single Re filaments. Lead was loaded in silica gel on single zone-refined Re filaments. Both U and Pb were analyzed in single-collector peak-switching mode using a Daly ion-counting system. In-run U fractionation was calculated based on the measured value for  $^{233}\text{U}$ / $^{236}\text{U}$  in the spike, and Pb fractionation was estimated to be 0.15%/amu based on replicate analyses of NBS 981. Data processing and age calculations were completed using the applications Tripoli and U-Pb Redux (Bowring et al., 2011; McLean et al., 2011). Decay constants used were  $^{238}\text{U} = 1.55125 \times 10^{-10}\text{a}^{-1}$  and  $^{235}\text{U} = 9.8485 \times 10^{-10}\text{a}^{-1}$  (Steiger and Jäger, 1977). All  $^{206}\text{Pb}$ / $^{238}\text{U}$  ages were corrected for U/Th disequilibrium using whole-rock U/Th ratios (Gaynor, 2018).

## RESULTS

### Geology of the Questa Mo Porphyry Deposit

Cross sections and analyses of the Questa deposit focused on the ore-forming intrusions and associated alteration (Figs. 5–8; Tables 2–4). Consequently, all pre-mineralization Precambrian rocks and Cenozoic volcanic rocks are undifferentiated on the sections. Three-point solutions of surveyed drill holes and intercept data were used to determine that the average orientation of the roofs of felsic intrusions within the southwest ore zone is 215°, 10° ( $n = 86$ ; right-hand rule). Faults observed in drill core and subsurface mapping are N-S-striking, high-angle normal faults. Argillic alteration and brecciation are common surrounding these high-angle normal faults. Low-angle faults were previously documented above the roof of the intrusive porphyries in the southwest ore zone (Meyer 1991; Ross et al., 2002). We identified another series of low-angle normal faults higher upsection above the northeast ore zone (Fig. 6). However, none of the low-angle faults were observed cutting any intrusions.

### Intrusive Rocks

Analysis of syn-mineralization and post-mineralization magmas identified eight mappable units as distinguished by groundmass, the abundance and size of phenocrysts, and crosscutting relationships (Figs. 9 and 10; Tables

3 and 4). We note, however, that interpreting changes in texture does not strictly require separate intrusive events. Instead, we describe each of these as discrete units on the basis of consistent crosscutting relationships and name them on the basis of their relevance to historic subsurface exploration at the mine. Crosscutting relationships indicate that the units from oldest to youngest are central aplite and northeast porphyry, pit porphyry, dark-matrix porphyry, southwest porphyry, Questa granite porphyry, post-mineralization dikes, and the equigranular granite. However, the oldest intrusive unit was not definitively determined; it is either the central aplite or the northeast porphyry. These units are not observed in contact with each other in any existing core, have similar phenocryst assemblages, and are older than any other intrusive unit with which they are in contact. Many of the rock units have sharp internal contacts between bodies of the same unit (e.g., southwest porphyry in the vein zone orebody; Figs. 5–8; Supplemental Items B-DD<sup>1</sup>); therefore, some map units (e.g., northeast porphyry, dark-matrix porphyry, southwest porphyry, and post-mineralization suite) include multiple separate bodies of similar mineralogy, texture, alteration, and relative age. Additionally, magmatic-hydrothermal breccia (MHBX) is distinguished on cross sections. This unit variably includes clasts of all pre-mineralization and syn-mineralization map units.

### Central Aplite

The central aplite (Fig. 9A) is a fine- to medium-grained porphyritic rock distinguished by low (<10%) phenocryst abundances of dominantly subhedral to anhedral plagioclase and K-feldspar crystals (Tables 3 and 4). It is an ~50–125-m-thick sheet and is present throughout the southwest ore zone. The roof of this intrusion dips gently to the north-northeast, and the lower portion of the unit is truncated by younger intrusions. Therefore, the lower contact of the central aplite was not fully observed in this study. The central aplite underlies and partially overlaps a zone of low-grade ( $\leq 0.10$  wt% MoS<sub>2</sub>), disseminated, and vein-style mineralization throughout the central deposit. MHBX bodies are commonly found above this intrusion but do not always host economic mineralization. Tabular pegmatite bodies occur inside the central aplite, correlate between drill holes, and are roughly parallel to the uppermost contact of the unit. Central aplite structurally above these pegmatite bodies hosts pervasive crosscutting vein alteration. Drill-hole data suggest that the bulk of the central aplite lies between the southwest and northeast ore zones, occupying the middle of the central deposit “horse-shoe” outline (Figs. 2 and 7).

### Northeast Porphyry

The northeast porphyry (Fig. 9B) is distinguished by faceted quartz phenocrysts, subhedral K-feldspar phenocrysts, and rare plagioclase phenocrysts.

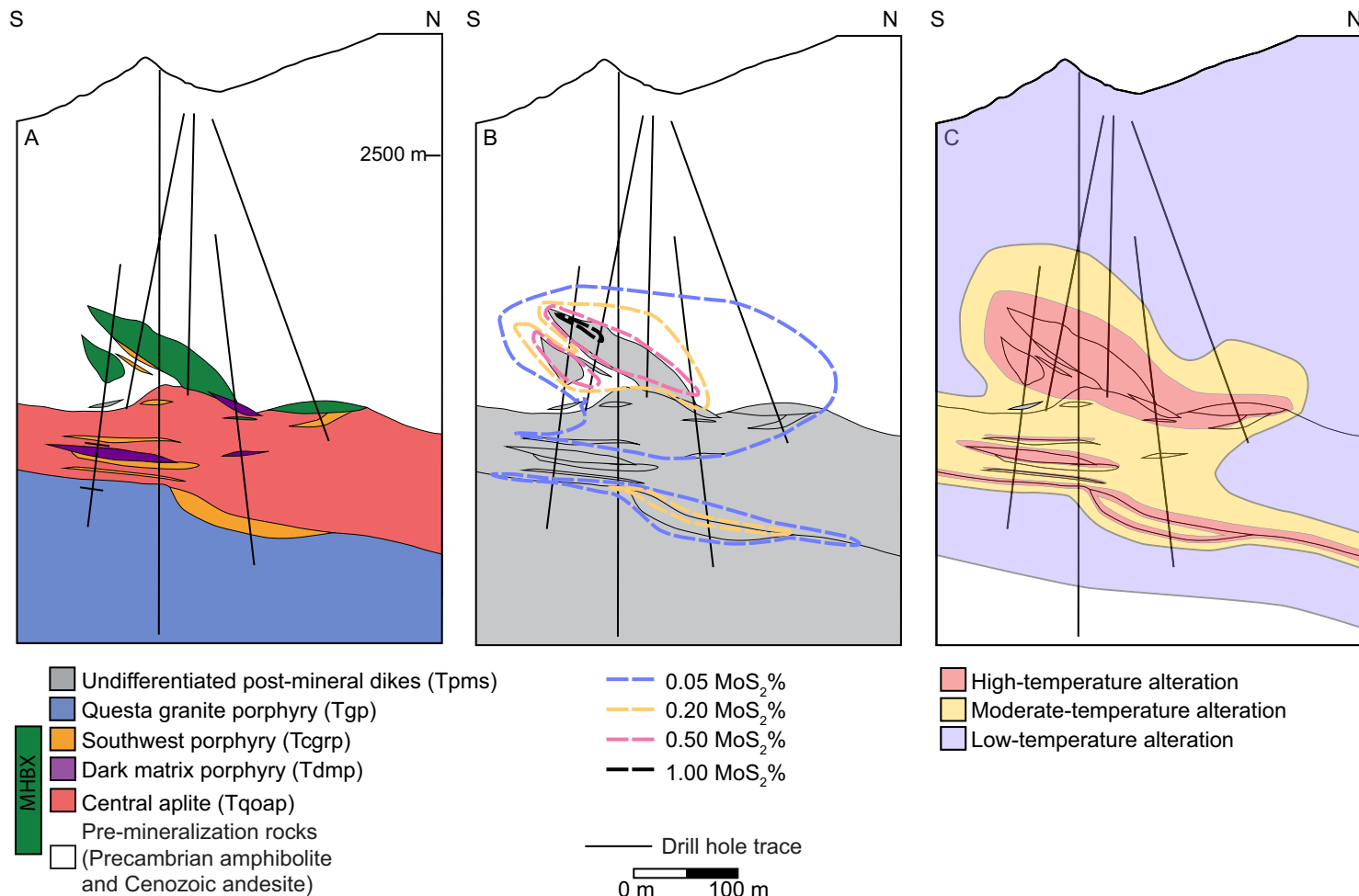


**Figure 5.** N-S Section 49600, showing the subsurface features of the southwest extension orebody (no vertical exaggeration; see Fig. 2 for location of cross section within the central deposit). All panels show the same geology but highlight different aspects: (A) geologic units, (B) molybdenite ore, and (C) hydrothermal alteration. The southwest extension orebody is composed of magmatic-hydrothermal breccias (MHBX) formed following the emplacement of the central aplite that was subsequently altered and mineralized by crosscutting intrusions of the dark-matrix porphyry and southwest porphyry. Dikes of the post-mineralization suite are barren and cut ore grade (a single dike is shown beneath MHBX bodies). Tick marks on southern drill trace in panel A indicate the location of Figure 13.

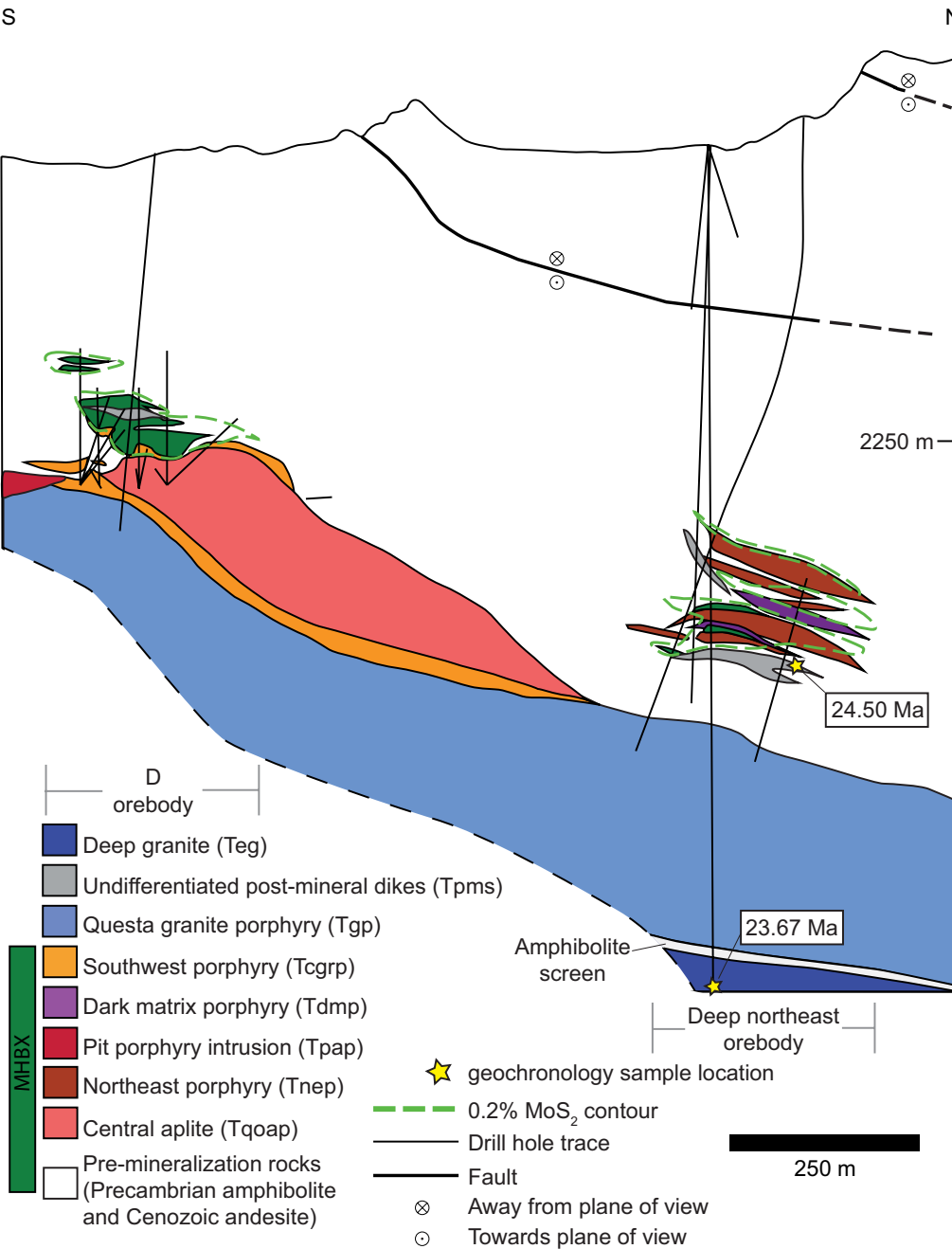


Figure 6. N-S Section 52000, showing the geology of the deep northeast and D-orebodies (no vertical exaggeration). The D-orebody is composed of magmatic-hydrothermal breccias (MHBX) formed following the emplacement of the central aplite. This breccia was later altered and mineralized by crosscutting intrusions of the pit porphyry and the southwest porphyry. The deep northeast orebody was assembled by a dike swarm of the northeast porphyry and dark-matrix porphyry. This area has significantly less exploratory drilling, and the abundance of mineralizing dikes in this section is underrepresented because most dikes are thin (<5 m). Stars indicate the sample location of DNE-5-3051, a barren dike of the post-mineralization suite (projected into the section) and sample DNE-1-3905 (deep granite). Ages shown are our preferred U-Pb ages (see text for discussion).

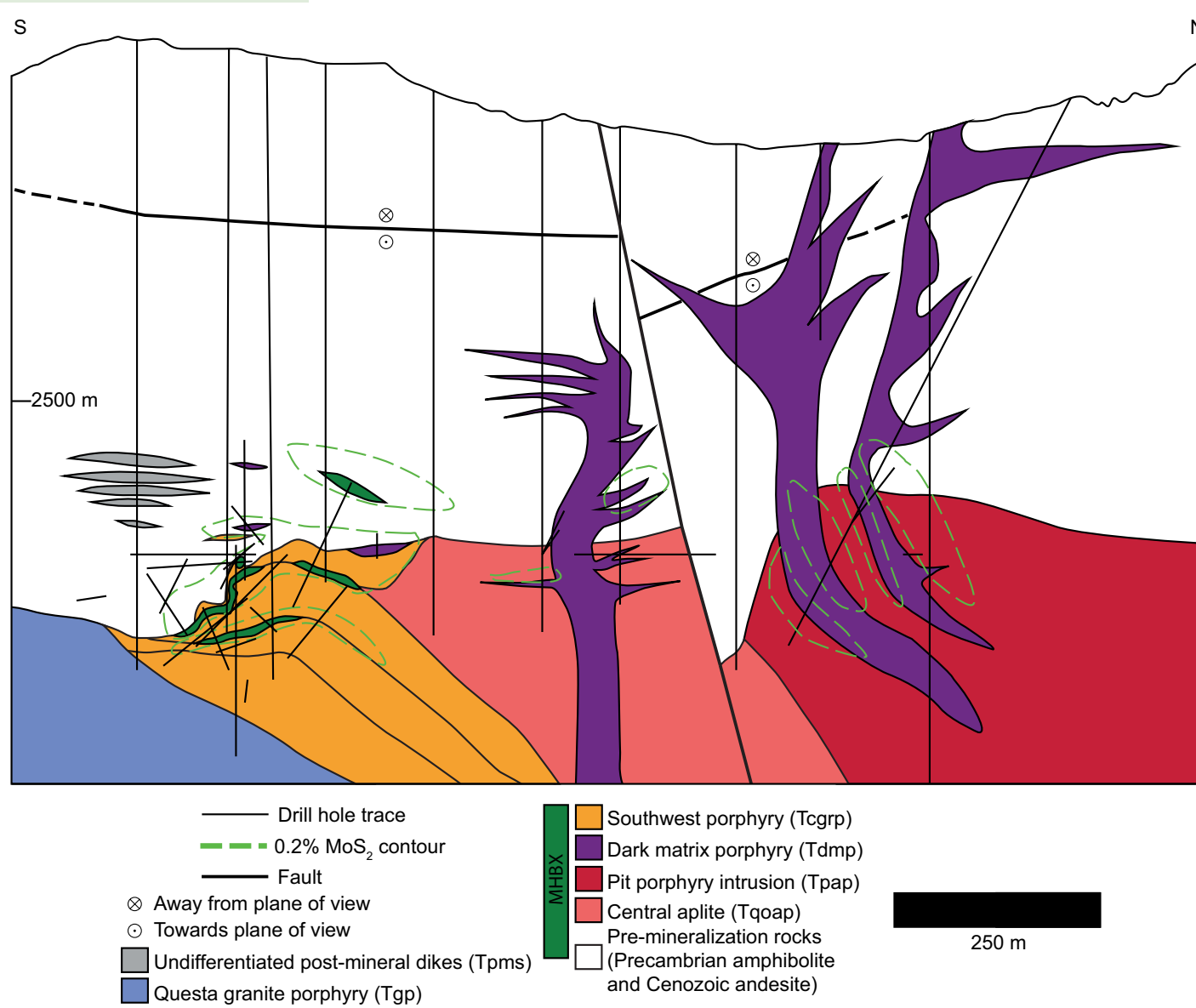
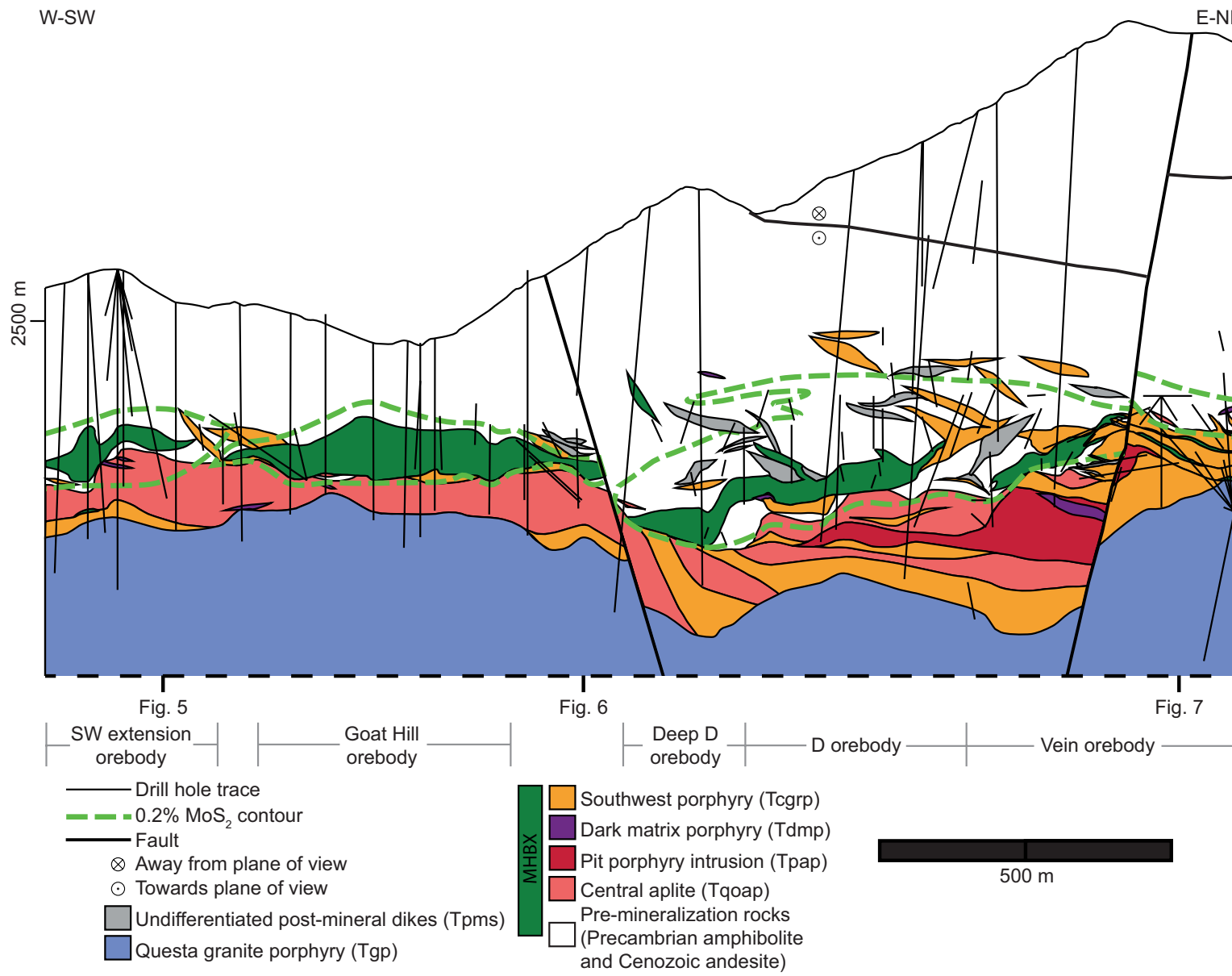


Figure 7. N-S Section 55200, showing the geology on the eastern side of the pit ore zone and the vein zone orebody and intrusions (no vertical exaggeration). Mineralizing intrusions in the pit ore zone (northern portion of section) are dominantly large sheets of the pit porphyry intrusion cut by Christmas-tree laccoliths of the dark-matrix porphyry and minor barren dikes. Christmas-tree laccolith structures observed in cores are similar to structures observed in the excavated pit sidewalls. In the vein zone orebody on the southern side of this section, the southwest porphyry is interpreted as four individual sills that amalgamate in a downward-stacking pattern. The relative age relationship is established by brecciation of early sills by later intrusions, local brain-rock textures, and local assay spikes in Mo. Mineralization within the vein zone orebody is mainly associated with the southwest porphyry, which did not generate significant magmatic-hydrothermal breccias (MHBX) and is instead focused largely in veins.



**Figure 8.** SW-NE cross section of the Questa Mo deposit, oriented roughly along the strike of the southwest ore zone and the same section as in Figure 3 (no vertical exaggeration; intersection lines of the N-S cross sections shown in Figs. 5–7 are indicated). Ore grade is discontinuous between many of the individual orebodies. The southwest ore zone includes a sheet of central aplite dissected by later intrusions of the pit porphyry intrusion, dark-matrix porphyry, and southwest porphyry. Magmatic hydrothermal breccias (MHBX) bodies with high-grade ore have multiple events of brecciation, alteration, and mineralization, indicating the overlapping mineralization was the result of distinct magmatic-hydrothermal events throughout deposit formation.

TABLE 3. MINERALOGY OF THE INTRUSIVE UNITS OF THE QUESTA MOLYBDENUM DEPOSIT

Geologic unit	Phenocrysts										Groundmass (mm)
	Quartz		K-feldspar		Plagioclase		Biotite		Amphibole		
	(%)	(mm)	(%)	(mm)	(%)	(mm)	(%)	(mm)	(%)	(mm)	
Equigranular granite (Teg)	10–20	0.5–7	30–50	2–7	15–25	0.5–4	1–3	0.5–4	1–2	1–3	n/a
Postmineralization suite (Tpms)*	V	V	V	V	V	V	V	V	V	V	V
Questa granite porphyry (Tgp)	3–5	3–7	2–7	3–8	0.1–2	2–4	0–1	1	–	–	0.7–1
Southwest porphyry (Tcgrp)	7–10	2–4	2–10	3–5	0–5	1–4	0–3	<0.1–1	–	–	<0.1–0.5
Dark-matrix porphyry (Tdmp)	0.5–5	2–3	5–15	4–8	2–15	2–4	1–3	1.5–3	0–1	2–3	<0.1–0.2
Pit porphyry intrusion (Tpap)	1–5.5	2–5	1–12	2–4	0–3	1.5–3	0–3	0.7–2	0.5–1.5	0.5–1.5	<0.1–0.5
Northeast porphyry (Tnep)	2–6	3	5	4	0.5	3	1	1	–	–	0.2
Central aplite (Tqoap)	0.5–2.5	2–3	0.2–3	2–6	0.1–2	2–5	0–1	1	–	–	<0.1–1.0

\*The postmineralization suite is compositionally diverse and does not have consistent phenocryst assemblages throughout the study area. All phases are variably present. V indicates that the phase is not present.

This porphyry is concentrated in the northeast ore zone and occurs as a series of stacked 2–35-m-thick sills separated mainly by andesite that hosts high- to moderate-temperature stockwork veins (Fig. 7). The northern extent of the unit is poorly determined due to limited drill-hole data. The northeast porphyry is spatially associated with high-grade ore in the deep northeast orebody, as well as 5–10-m-thick MHBX bodies.

### Pit Porphyry

The pit porphyry (Fig. 9C) is an asymmetric sheet and series of dikes distinguished by 8%–25% phenocrysts of quartz, feldspars, biotite and amphibole, and a gray, typically sugary, groundmass (Tables 3 and 4). The porphyry is defined by exposures in the southwest, pit, and northeast orebodies. The roof of the pit porphyry is a distinct mostly aphyric aplite that gently grades downward to a porphyritic aplite. The aphyric top of the pit porphyry intrusion is thin (<5 m thick) and observed sparingly in the vein zone orebody. It is too thin to represent as a separate unit on the cross sections. This unit underlies and partially hosts low-grade Mo vein mineralization in the pit ore zone. The pit porphyry pinches out and dips to the northwest toward the southwest and northeast ore zones. It is structurally beneath ore-grade mineralization (0.2 wt% MoS<sub>2</sub>) in the southwest ore zone (Figs. 5–8).

### Dark-Matrix Porphyry

The dark-matrix porphyry is characterized by its dark groundmass color, the presence of biotite, amphibole, and magnetite phenocrysts and large feldspar phenocrysts (0.5–6 cm) that may have rapakivi textures (Tables 3 and 4; Fig. 9D). This unit formed numerous stacked sheets in the northeast and southwest ore zones and vertically extensive Christmas-tree laccoliths near

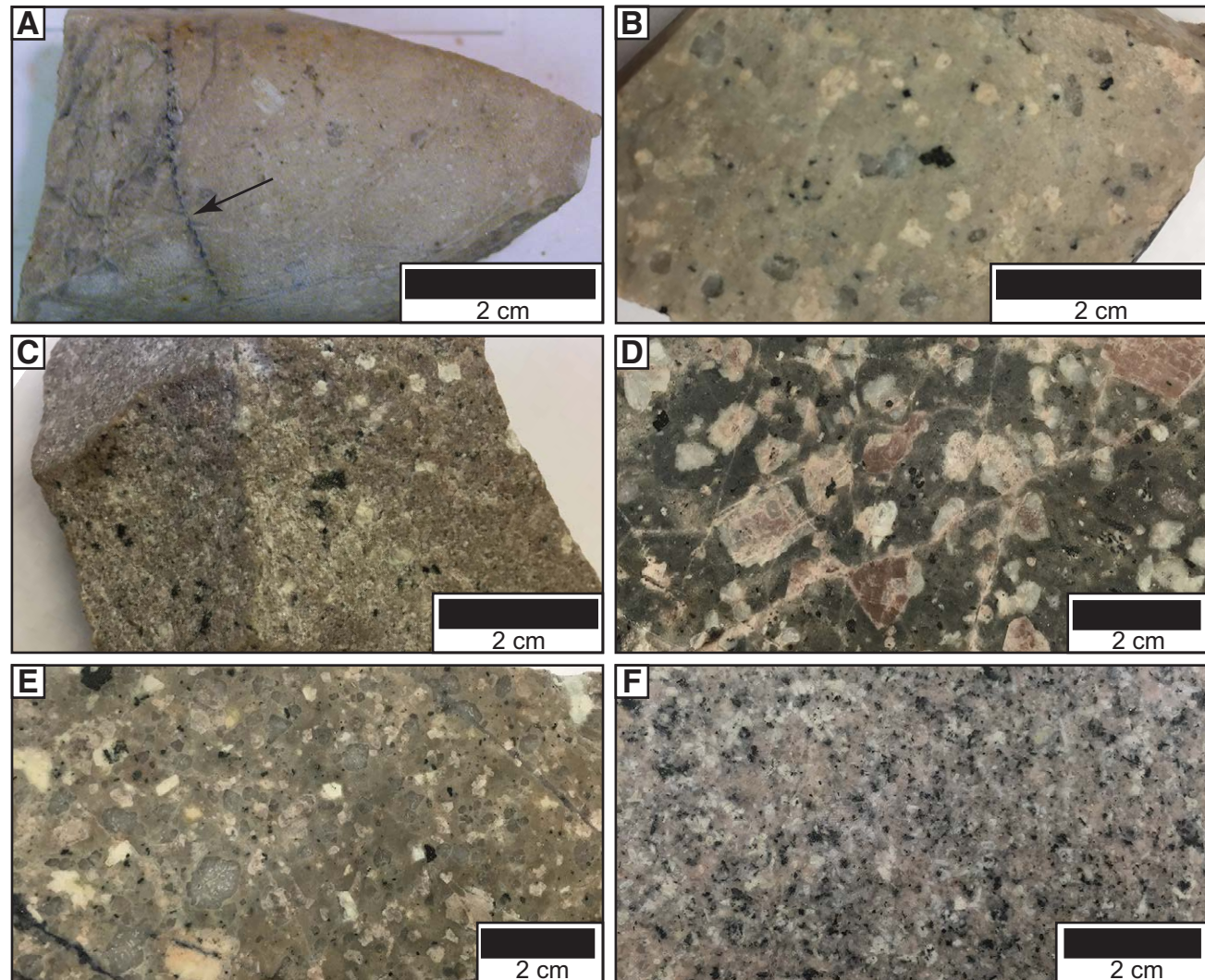
the pit ore zone (Fig. 7). Composite quartz-molybdenite veins and stockwork Mo-bearing veins are abundant in the wall rock near this porphyry and are associated with high-grade mineralization ( $\geq 0.20$  wt% MoS<sub>2</sub>). Christmas-tree laccoliths of the dark-matrix porphyry cut the pit porphyry intrusion in the F<sub>2</sub> orebody and continue higher upsection into the andesite wall rocks. Dikes of the dark-matrix porphyry cut the central aplite, pit porphyry intrusion, and northeast porphyry in the northeast and southwest ore zones. Horizontal exploration cores (Fig. 7) and exposure along the old pit wall verify that sheets of dark-matrix porphyry exposed there have a common feeder. The roofs of thin sheets of the dark-matrix porphyry occasionally contain altered clasts of the central aplite and pit porphyry intrusions (Fig. 4B).

### Southwest Porphyry

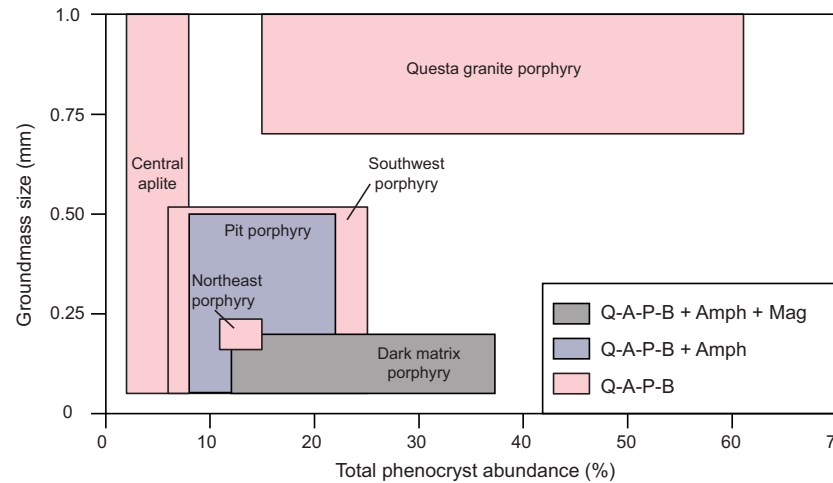
The southwest porphyry underlies much of the high-grade vein mineralization that was targeted during underground mining of the southwest ore zone. This unit is distinguished by a pink to tan, fine-grained to aplitic groundmass and abundant subhedral quartz phenocrysts (7%–10%; Tables 3 and 4; Fig. 9E). Chilled margins within the southwest porphyry are common, and fining of phenocryst size combined with potassic alteration along the roof of intrusive sheets of southwest porphyry make the unit appear similar to the central aplite. Delineation between units at these contacts was significantly aided by the presence of MHBX bodies and brain-rock textures. In many cases, rocks with brain-rock texture underlie thin MHBX bodies. Because it underlies much of the high-grade mineralization and contains traceable layers of brain rock and MHBX (e.g., indicative of volatile cycling), we present the southwest porphyry as a set of 5–45-m-thick stacked sheets separated by MHBX bodies within the vein zone orebody (e.g., Figs. 7 and 8). To the west, these sheets become vertically discontinuous with screens of central aplite or volcanic rock between textural units (Fig. 8).

TABLE 4. HAND-SAMPLE DESCRIPTIONS OF GEOLOGIC UNITS OF THE QUESTA MOLYBDENUM DEPOSIT

Geologic unit	Hand-sample description	Alteration textures
Equigranular granite (Teg)	Coarse-grained, relatively equigranular granite. Grains are interlocking, without any significant groundmass. Rapakivi grains present but uncommon relative to feldspars lacking compositional zoning.	Mild low-temperature veins present at the roof of the intrusion (calcite ± fluorite); no moderate- to high-temperature alteration observed.
Postmineralization suite (Tpms)	A compositionally diverse suite of dikes, ranging from latite to rhyolite, identified by cutting Mo grade and alteration haloes and therefore postdating mineralization. Textures range from fine grained to aplitic and equigranular to porphyritic. Few magmatic breccias present and lack the alteration mineralogy observed in the magmatic-hydrothermal breccia (MHBX), more similar to clastic dikes.	Occasionally associated with barren high-temperature alteration above ore zones (e.g., silicified); however, most commonly cutting altered rock.
Magmatic-hydrothermal breccia (MHBX)	Altered clasts of both andesite and plutonic rocks encased within a matrix of magmatic-hydrothermal alteration minerals. Breccias within the vein zone and southwest extension orebodies contain breccia clasts of previous breccias, indicative of multiple distinct breccia formation events.	Andesite clasts typically altered to biotite and often overprinted by moderate-temperature sericite-pyrite. Rhyolite porphyries typically flooded with K-feldspar. Detailed description of MHBX at Questa can be found in Ross et al. (2002).
Brain rock	Textural unit found within multiple intrusive units associated with mineralization, composed of banded layers of crenulate quartz and alkali feldspar and commonly interfingered or interleaved with aplite or pegmatite. Accessory minerals of fluorite, biotite, or phlogopite can be concentrated within the margins of layers. Most commonly observed within the southwest porphyry (Tcgrp) and central aplite (Tqoap).	Not applicable.
Questa granite porphyry (Tgp)	Pink to salmon-colored groundmass; quartz phenocrysts are subhedral hexagonal to square, although occasionally anhedral; K-feldspar phenocrysts are euhedral to subhedral rectangular prisms; plagioclase feldspars are subhedral to anhedral square grains, with occasional grain boundary rounding. Fine-grained aplite phase found at roof coarsens downward into main body over 5–10 m gradational contact.	Mild quartz ± molybdenite veining within the cap of the unit, mostly restricted to the aplite phase. Structurally deeper portions of the pluton host little to no alteration.
Southwest porphyry (Tcgrp)	Pink to tan fine-grained to sugary groundmass; abundant quartz phenocrysts are subhedral and square to hexagonal; K-feldspar phenocrysts are anhedral, with smaller phenocrysts subhedral and rectangular; plagioclase phenocrysts are subhedral and square; biotite is trace to uncommon and ranges from euhedral books to plate grains; total phenocrysts range from 10%–25%.	Mild to weak sericite alteration is present throughout much of the unit; however, alteration is moderate to high temperature along fracture planes locally. Structurally higher bodies are more commonly cut by high-temperature alteration phases. Roofs of southwest porphyry are commonly local dense networks of quartz-molybdenite veins.
Dark-matrix porphyry (Tdmp)	Dark-gray to purple groundmass ranging from aphanitic to fine grained; quartz phenocrysts range from subhedral and hexagonal to anhedral and orbicular; alkali feldspar phenocrysts are euhedral to subhedral and commonly display rapakivi textures; biotite phenocrysts are subhedral books; elongate, prismatic to needle-like amphibole phenocrysts present; euhedral magnetite present up to 4%, but commonly 1.5%; typically 8%–35% total phenocrysts.	Sericite alteration commonly fills fractures cutting previous high- and low-temperature veins; strong potassic alteration observed in the form of biotite alteration of groundmass and K-feldspar envelopes surrounding veins. The most significant alteration of Tdmp is observed in the southwest extension and vein zone orebodies.
Pit porphyry intrusion (Tpap)	Dark-gray to purple groundmass with a sugary texture; typically 9%–22% phenocrysts present; gradational contact with an aphyric cap present in the eastern portion of the study area; hosts occasional pods that are rich in biotite and hornblende, usually located near upper portion of the unit.	Pervasive high- to moderate-temperature alteration present through much of the unit. Potassic flooding is common surrounding quartz and potassium feldspar alteration veins. Moderate-temperature sericite veins present as well at a lower abundance than high-temperature alteration veins. Alteration strongest local to contacts with Tcgrp.
Northeast porphyry (Tnep)	Pink to light-gray groundmass with fine-grained texture; quartz phenocrysts are light gray and tend to be faceted; K-feldspar phenocrysts are subhedral to anhedral and uncommonly range up to 10 mm and sometimes host biotite inclusions; biotite phenocrysts are subhedral to anhedral; typically less than 15% total phenocrysts.	Alteration tends to be focused to the intrusive roofs, with veins emanating outward; commonly hosts quartz-molybdenite and K-feldspar alteration veins, both of which locally disseminate alteration in an envelope around fractures; weak clay alteration present in some locations; which postdates all other alteration when present; alteration most common near contacts with Tdmp.
Central aplite (Tqoap)	Light-pink to dark-gray, fine- to medium-grained groundmass; quartz phenocrysts subhedral and hexagonal; K-feldspar phenocrysts subhedral to anhedral rectangular prisms; plagioclase feldspars are subhedral to anhedral; biotite phenocrysts are uncommon, platy, and anhedral when present; typically less than 10% total phenocrysts.	Pervasive silicic and potassic alteration common throughout unit; commonly pervasive sericite present. Plagioclase phenocrysts altered to clays. Also cut by lower-temperature alteration veins (e.g., fluorite and calcite). Numerous moderate- to high-temperature alteration assemblages observed cutting moderate- to low-temperature veins.



**Figure 9.** Representative hand sample and drill core for intrusions at the Questa Mo deposit, in relative age order from oldest to youngest. Detailed rock descriptions can be found in Tables 3 and 4. (A) Central aplite has a low phenocryst content (<10%), subhedral to anhedral plagioclase and K-feldspar phenocrysts, and a light-pink to gray groundmass. The quartz-molybdenite vein cutting this sample (indicated by arrow) was dated with Re-Os methods to  $24.760 \pm 0.026$  Ma (sample AR98 of Rosera et al., 2013). (B) The northeast porphyry (DNE-2 2153). (C) The pit porphyry intrusion is one of the few intrusive units with both biotite and amphibole phenocrysts. Sample dated with U/Pb zircon geochronology at  $24.91 \pm 0.07$  Ma (Rosera et al., 2013) (OM11-01). (D) The dark-matrix porphyry has a dark-colored groundmass, feldspar phenocrysts that commonly display rapakivi textures, and amphibole, biotite, and magnetite phenocrysts. Sample dated in this study (DD-9-645;  $24.74 \pm 0.36$  Ma). (E) The southwest porphyry (VN38 935). (F) The Questa granite porphyry.



**Figure 10.** Total phenocryst abundance versus groundmass for porphyritic intrusive rocks at the Questa deposit. Groundmass and modal phenocryst data from Table 3. Units are classified based on phenocryst assemblage, texture, and field relationships. Abbreviations: Q—quartz; A—alkali feldspar; P—plagioclase; B—biotite; Amph—amphibole; Mag—magnetite.

### Questa Granite Porphyry

The Questa granite porphyry, distinguished by a pink to salmon, coarse-grained groundmass (0.7–1.0 mm) and abundant prismatic K-feldspar phenocrysts (Fig. 9F; Tables 3 and 4), underlies the entire central deposit (Figs. 5–8). Like the pit porphyry, the Questa granite porphyry has a downward coarsening texture. In some locations within the northeast ore zone, the porphyry underlies an ~15-m-thick zone of sub-economic (<0.20 wt% MoS<sub>2</sub>) mineralization; however, in most exploratory drilling, the Questa granite porphyry is associated with <10 m of non-economic mineralization (generally, <0.10 wt% MoS<sub>2</sub>). Small areas of low-grade mineralization were observed in the southwest extension orebody (Fig. 5). Wall rock above this porphyry commonly has silicic and argillic alteration, typically in the form of barren vein alteration. The shape of the Questa granite porphyry at depth is uncertain because the low-grade nature of Mo mineralization associated with this unit did not warrant significant exploration at depth. However, one vertical drill hole in the deep northeast exploratory program intercepted relatively flat-lying (~10° dip observed in core) screen of Precambrian amphibolite (Fig. 6). The Questa granite porphyry cuts the central aplite and the dark-matrix porphyry underground in the vicinity of the Goat Hill ore block, the pit porphyry within the pit ore zone, and the southwest porphyry in the vein orebody.

### Post-Mineralization Suite

The post-mineralization suite cuts all earlier intrusions and includes compositionally diverse (latite to rhyolite) barren dikes. Post-mineralization dikes

are undifferentiated and are shown as a single set of dikes even though field relations require that multiple generations are present. Cross sections only show dikes greater than 10 m thick; as a result, the complexity of intrusive relationships in cross section is underrepresented in regions containing dike swarms (e.g., southwest extension, Fig. 5; deep northeast, Fig. 6). Dikes of this suite cut the central aplite, northeast porphyry, pit porphyry intrusion, dark-matrix porphyry, and southwest porphyry. Some of these dikes cut the Questa granite porphyry; however, many are structurally separated from it.

### Deep Granite

A barren “deep granite” (Teg; Fig. 6) is distinguished by an equigranular texture and composed predominately of quartz and two feldspars (Tables 3 and 4). The granite was intercepted in an exploration hole in the northeast ore zone. This unit lacks significant alteration and is coarser grained than the intrusive units structurally above it. It is separated from the Questa granite porphyry by an ~15-m-thick screen of Proterozoic amphibolite.

### Magmatic-Hydrothermal Breccia (MHBX)

Magmatic-hydrothermal breccia bodies identified herein are similar to those described by Ross et al. (2002). Bodies of MHBX range from 0.25 to 100 m in structural height and are composed of clasts of igneous rocks (andesite, central aplite, northeast porphyry, pit porphyry, dark-matrix porphyry, and southwest porphyry) encased within veins ranging from quartz-molybdenite to

calcite-fluorite in composition (Fig. 4C). The Questa granite porphyry, post-mineralization dikes and equigranular granite have not been observed as clasts within MHBX. High-intensity veining surrounding MHBX bodies is common, with vein abundance decreasing significantly with increasing distance away from breccia bodies.

Large-scale breccias are located above the southwest ore zone within andesite wall rock and are discontinuous along strike of the ore body (Fig. 8). Smaller-scale MHBX bodies (<5 m) are found at the contacts between felsic intrusive sheets of the deposit and commonly contain only clasts of the wall rock structurally above them (e.g., MBX above southwest porphyry intrusions in Fig. 8). In the southwest extension and vein zone orebodies, individual breccia clasts contain clasts of previous magmatic-hydrothermal breccias. Breccia clasts are commonly encased by high-temperature veins that cut both the clast and its older veins (e.g., Fig. 4B).

### Alteration in the Questa Mo Porphyry Deposit

Observations of alteration of the Questa deposit, both from historical studies and this work, were organized on the basis of previous geological and microthermometry studies (Table 2, references therein). High- and high- to moderate-temperature alteration veins (quartz-molybdenite, K-feldspar-biotite, biotite, K-feldspar-quartz, and K-feldspar-magnetite) range in thickness from 0.1 to 5 cm and occur as both simple and composite veins throughout the deposit. Regions of this alteration range from 0 to 10 m vertically above intrusive contacts when not associated with MHBX bodies and where proximal to felsic intrusions. Some veins have envelopes of either quartz, K-feldspar, or sericite alteration surrounding sharp vein contacts (Fig. 4D). Quartz-molybdenite veins in the subsurface workings have an average orientation of 245°, 60° ( $n = 668$ ), which is 50° from the average orientation of roof contacts of intrusions in the southwest ore zone (Fig. 11). High- and high- to moderate-temperature alteration veins were observed cutting moderate- and low-temperature veins in the deep northeast, southwest extension, and vein zone orebodies.

Low-temperature vein alteration is dominated by fluorite, calcite, and anhydrite and is observed both proximal and distal to felsic intrusions (>350 m). Low-temperature veins are observed cutting high-, high- to moderate-, and moderate-temperature veins, as well as similar composition low-temperature veins. Disseminated pyrite mineralization (defined by 0.5%–10% pyrite modally within a rock) occurs structurally above all studied ore blocks and, in map view, is discontinuous away from ore zones. Pyrite mineralization is observed in drill-core and subsurface operations and extends to the surface where it correlates with hydrothermal alteration scars. These pyrite mineralization zones begin ~20–50 m above the roofs of felsic intrusions and range from 30 to 250 m in height.

Recent drilling in the vein zone orebody focused on regions hosting brain rock, and our analysis shows that bodies of brain rock are commonly continuous across offset drill holes and occur subparallel to zones of high  $\text{MoS}_2$

grades and intrusive-contact breccias. This is exemplified in the southwest extension mine block (Fig. 5), where previous studies lumped intrusive rocks into only a few units. Magmatic-hydrothermal breccias, pegmatite bodies, and unidirectional solidification textures within this region project between drill holes. Breccias and unidirectional solidification textures commonly parallel changes in the phenocryst abundances and size within the southwest porphyry and Questa granite porphyry, both increasing structurally lower (e.g., Fig. 5).

### Zircon Geochronology

We present U/Pb zircon TIMS data for three of the rock units described above. We selected samples of dark-matrix porphyry, postmineral rhyolite, and the deep granite. We dated the dark-matrix porphyry because crosscutting relationships suggest it is intermediate in age relative to previously dated units (it cuts the pit porphyry and is cut by the Questa granite porphyry; Rosera et al., 2013). The postmineral rhyolite was selected to better determine when mineralization at Questa ended. Finally, the equigranular granite was selected to test the possibility that it was a larger magma body that supplied volatiles and metals to the overlying ore zone. All zircon U/Pb ages are concordant within analytical and decay constant uncertainties, although the age spectra of given samples are complicated (Table 5; Fig. 12).

Sample DD-9-651 was of a dike of the dark-matrix porphyry cutting the central aplite and pit porphyry, located 1.6 m below the dike's contact with central aplite (Fig. 4B).  $^{206}\text{Pb}/^{238}\text{U}$  ages of individual zircon grains range from 24.88 to 24.52 Ma, with five of seven analyzed grains clustering around 24.77 Ma. Radiogenic Pb abundances from grains analyzed from this sample were consistently low, leading to high uncertainty for individual analyses.

A sample of the post-mineralization suite (DNE-5-3051) was collected from a rhyolite dike cutting mineralization and the dark-matrix porphyry in the deep northeast orebody (Fig. 6).  $^{206}\text{Pb}/^{238}\text{U}$  ages for individual zircon grains range from 24.69 to 24.49 Ma, with four grains overlapping within uncertainty at 24.50 Ma and two older grains (24.69 and 24.58 Ma).

A sample of the deep granite (DNE-1-3905) was collected from a deep exploratory drilling in the deep northeast orebody (Fig. 6). Individual zircon grains yield  $^{206}\text{Pb}/^{238}\text{U}$  ages ranging from 23.90 to 23.27 Ma, with five grains overlapping within uncertainty at 23.70 Ma, two older grains (23.90 and 23.74 Ma), and one younger grain (23.27 Ma).

### DISCUSSION

A detailed reevaluation of the intrusive history of the Questa Mo deposit yields new insight into its complexity. Integrating these insights with new and previously published zircon geochronologic data permits better understanding of the assembly of the deposit and implications for the evolution of Climax-type Mo porphyry systems.

## Age of Intrusions within the Central Deposit

The zircon age spectra for the samples dated in this study span a range beyond analytical uncertainty of individual analyses (Fig. 12). There are multiple models to interpret such spectra, which are increasingly recognized in plutonic rocks as analytical techniques improve (Samperton et al., 2015; Schaltegger and Davies, 2017): (1) the youngest grain is the only age that reflects crystallization at the emplacement level, whereas older grains are antecrystic (e.g., Schaltegger et al., 2009); (2) the spectrum reflects the full period of crystallization of a magma (e.g., von Quadt et al., 2011; Wotzlaw et al., 2013); (3) the spectrum is complicated by old antecrystic grains and Pb loss potentially yielding geologically meaningless ages. Interpretation of the age spectra, therefore, requires independent observations. Herein, we present multiple interpretations of the age spectra and a “preferred” interpretation with our rationale. In each case, the preferred interpretations do not significantly alter the age, but do narrow

the uncertainty in the age. That is, regardless of whether the entire zircon population is interpreted to reflect magmatic growth (scenario 2), or some analyses are excluded from the age calculation because they are interpreted to be antecrystic (scenarios 1 and 3), none of our interpretations based on the ages are impacted.

It is rather common to dismiss the impact of Pb loss on zircon age spectra because the thermal annealing–chemical abrasion technique employed in most labs (and this study) has proven highly effective at removing damaged volumes of zircon (Mundil et al., 2004; Mattinson, 2005; Schaltegger and Davies, 2017). Whereas this may be likely in relatively unaltered plutons, it is less likely the case in magmatic-hydrothermal systems with high-F activities, such as Climax-type deposits. Volcanic rocks that should have rapid, simple crystallization histories can still produce zircon age spectra featuring Pb loss after interaction with hydrothermal fluids (Ovtcharova et al., 2015; Schoene et al., 2015). Consequently, the young “tails” in the zircon age spectra from this

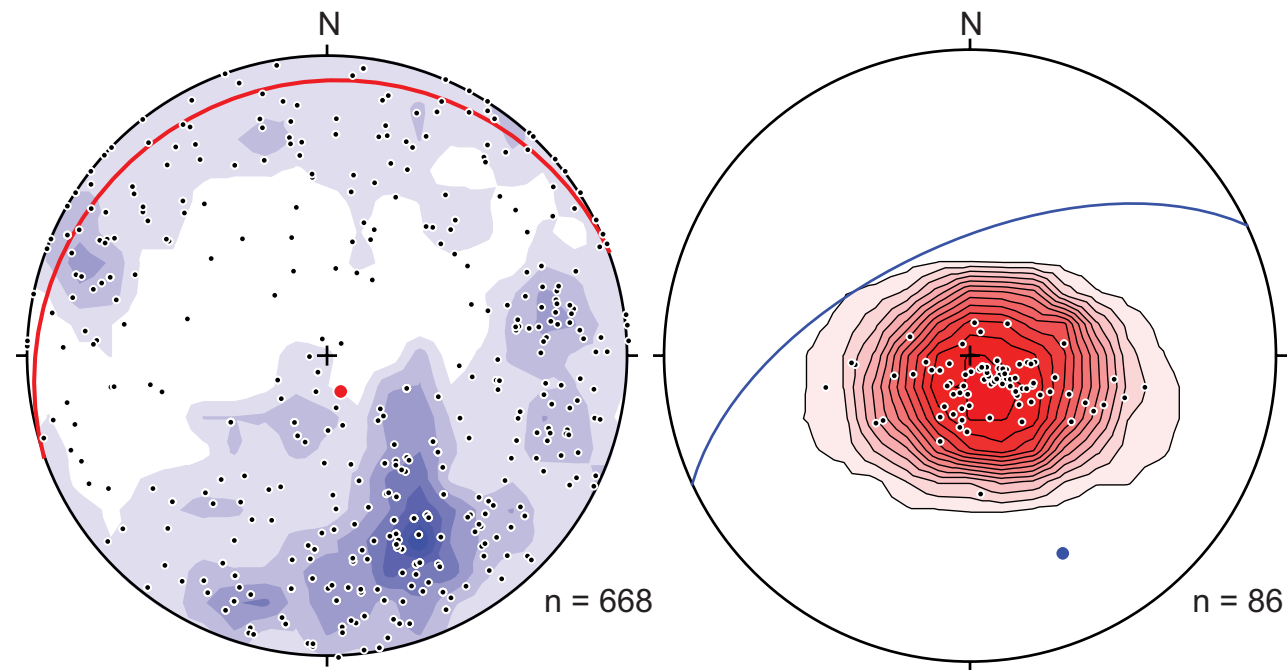


**Figure 11.** Lower-hemisphere, equal-area stereonet projections with  $2\sigma$  Kamb contours of the orientations of subsurface veins (A) and pluton roofs (B) found within the southwest ore zone. The angle between the average plane for these two data sets is  $50^\circ$ , suggesting that veins were formed from fluids exsolved from proximal intrusions. (A) Molybdenite-bearing vein orientations were measured in subsurface exposures and are plotted as poles to planes. These veins have an average plane orientation of  $245^\circ, 60^\circ$  ( $n = 668$ ), with Kamb contours shown in blue. The red plane and pole are the average intrusive roof orientations within the area that vein orientations were collected. (B) Orientation of the intrusive roofs within the southwest ore zone measured in the subsurface and estimated from cross sections plotted as poles to planes, with Kamb contours shown in red. The average planar orientation is  $215^\circ, 10^\circ$  ( $n = 85$ ). The blue plane and pole are the average molybdenite-bearing vein orientation in the subsurface.

TABLE 5. URANIUM-LEAD DATA FOR ROCKS OF THE QUESTA PORPHYRY MOLYBDENUM DEPOSIT

ID	Concentration			Ages (Ma) <sup>#</sup>						Total common Pb (pg)					
	U (ppm)	Pb* (pg)	Th <sup>†</sup> U	$\frac{^{206}\text{Pb}^{\$}}{^{204}\text{Pb}}$	$\frac{^{206}\text{Pb}^{\#}}{^{238}\text{U}}$	Error (%)	$\frac{^{207}\text{Pb}^{\#}}{^{235}\text{U}}$	Error (%)	$\frac{^{207}\text{Pb}^{\#}}{^{206}\text{Pb}}$	Error (%)	$\frac{^{206}\text{Pb}^{\#}}{^{238}\text{U}}$	Error (Ma)	$\frac{^{207}\text{Pb}^{\#}}{^{235}\text{U}}$	Correlation coefficient	
<i>DD-9-651** dark-matrix porphyry; deep D ore block (Th/U = 3.67)</i>															
F-1	71.5	1.29	0.810	53.74	0.003831	(1.5)	0.02690	(29)	0.05093	(27)	24.73	(0.37)	26.95	0.894	2.08
F-3	148	2.79	0.778	123.1	0.003797	(0.67)	0.02229	(129)	0.04257	(1)	24.52	(0.16)	22.38	0.840	1.53
F-4	203	3.72	0.855	165.1	0.003855	(0.44)	0.02523	(7.5)	0.04746	(7.2)	24.88	(0.11)	25.30	0.808	1.42
F-6	217	5.33	0.765	215.6	0.003834	(0.35)	0.02373	(6.4)	0.04489	(6.1)	24.76	(0.088)	23.82	0.815	1.55
F-7	341	3.76	0.816	172.7	0.003829	(0.43)	0.02348	(7.8)	0.04447	(7.4)	24.72	(0.11)	23.56	0.795	1.38
F-8	399	2.30	1.06	91.2	0.003801	(0.76)	0.02387	(17)	0.04554	(16)	24.53	(0.19)	23.95	0.872	1.69
F-11	324	3.61	0.77	143.5	0.003838	(0.51)	0.02271	(9.7)	0.04291	(9.3)	24.78	(0.13)	22.80	0.821	1.66
<i>DNE-5-3051** barren dike (Tpms); deep northeast ore block (Th/U = 2.81)</i>															
F-1	215	11.4	0.747	460.3	0.003807	(0.22)	0.02410	(2.7)	0.04591	(2.5)	24.58	(0.058)	24.18	0.671	1.49
F-9	204	2.72	0.761	199.5	0.003824	(0.38)	0.02431	(6.5)	0.04610	(6.2)	24.69	(0.095)	24.39	0.775	0.86
F-13	276	14.5	0.861	891.2	0.003793	(0.18)	0.02427	(1.4)	0.04641	(1.3)	24.48	(0.050)	24.35	0.581	0.93
F-20	391	31.9	0.793	537.8	0.003794	(0.19)	0.02452	(2.2)	0.04687	(2.0)	24.49	(0.052)	24.60	0.641	3.49
F-21	799	9.36	0.807	494.3	0.003795	(0.22)	0.02408	(2.4)	0.04602	(2.3)	24.50	(0.057)	24.16	0.528	1.12
F-24	1250	8.12	0.762	884.5	0.003794	(0.20)	0.02439	(1.6)	0.04662	(1.4)	24.49	(0.053)	24.46	0.600	0.54
<i>DNE-1-3905** deep granite (Th/U = 6.11)</i>															
F-1	1582	65.8	0.471	1400.6	0.003666	(0.14)	0.02366	(0.9)	0.04681	(0.8)	23.69	(0.033)	23.74	0.479	2.9
F-2	302	33.3	0.612	1439.2	0.003678	(0.17)	0.02357	(1.1)	0.04648	(1.0)	23.76	(0.040)	23.66	0.770	1.4
F-4	628	22.3	0.644	618.9	0.003665	(0.18)	0.02318	(2.1)	0.04587	(2.0)	23.68	(0.041)	23.27	0.649	2.2
F-5	1042	40.4	0.557	710.6	0.003680	(0.17)	0.02347	(1.7)	0.04625	(1.6)	23.78	(0.040)	23.55	0.578	3.5
F-6	978	26.2	0.531	2209.6	0.003661	(0.22)	0.02356	(0.7)	0.04668	(0.6)	23.65	(0.052)	23.65	0.573	0.7
F-8	536	28.9	0.548	830.8	0.003659	(0.16)	0.02348	(1.6)	0.04657	(1.5)	23.64	(0.039)	23.57	0.500	2.2
F-9	412	15.7	0.505	377.7	0.003666	(0.18)	0.02371	(3.1)	0.04692	(2.9)	23.69	(0.043)	23.79	0.776	2.7
F-10	431	8.9	0.796	251.0	0.003679	(0.27)	0.02381	(4.9)	0.04697	(4.6)	23.77	(0.065)	23.90	0.826	2.2

<sup>\*</sup>Radiogenic Pb.<sup>†</sup>Th contents calculated from radiogenic  $^{208}\text{Pb}$  and the  $^{207}\text{Pb}/^{206}\text{Pb}$  date of the sample, assuming concordance between U-Th and Pb systems.<sup>‡</sup>Measured ratio corrected for fractionation only. All Pb-isotope ratios were measured using the Daly detector and are corrected for mass fractionation using 0.15 %/amu.<sup>§</sup>Corrected for fractionation, spike, blank, and Th disequilibrium. All common Pb is assumed to be blank.<sup>\*\*</sup>Sample number refers to exploration drill-hole number (e.g., "DD-9") and downhole footage (e.g., "651" = 651').Note: All errors except error in the  $^{206}\text{Pb}/^{238}\text{U}$  age are reported in percent at the  $2\sigma$  confidence interval. Error in the  $^{206}\text{Pb}/^{238}\text{U}$  age is reported in absolute (Ma) at the  $2\sigma$  confidence interval.

study and earlier work on Questa (Rosera et al., 2013) could be the result of Pb loss related to circulation of F-rich hydrothermal fluids associated with later intrusions. However, we draw a distinction between "tails" of isolated grains yielding a spectrum of young ages (e.g., the Tgp samples from Rosera et al., 2013) and "plateaus" of consistent young ages (e.g., Tpms and Teg; Fig. 12). Whereas the former may reflect Pb loss, we are skeptical that multiple grains would experience precisely the same Pb loss necessary to give consistent ages.

The age spectrum for the dark-matrix porphyry is complicated. This is exacerbated by the small zircon grain size and low concentrations of radiogenic Pb (Table 5), resulting in unusually large uncertainties for these analyses. Consequently, a precise age interpretation is not possible. Regardless of zircon systematics (antecrysts, Pb loss, protracted growth, or all of these), the dark-matrix

porphyry cuts the pit porphyry (24.91 Ma; Rosera et al., 2013) and is cut by the Questa granite porphyry (24.53–24.44 Ma; Rosera et al., 2013), and the age data (24.88–24.52 Ma; Table 5) are consistent with these relationships. Therefore, we accept the weighted-mean age of all zircons from this sample as a reasonable estimate of the age of the dark-matrix porphyry, but we also acknowledge a large uncertainty in this age, conservatively accepting  $\Delta t$  between the oldest and youngest grains as a reasonable estimate ( $24.74 \pm 0.36$  Ma; Fig. 12).

The weighted mean and  $\Delta t$  (calculated as above) for all zircons from the barren dike (24.52;  $\Delta t = 0.20$  Ma) overlap with the weighted mean for the five youngest grains from this sample ( $24.50 \pm 0.02$  Ma). We suggest that the oldest grain from this sample may be antecrystic, and we accept the latter age and uncertainty as our preferred age for the barren dike sample. The ages for zircons

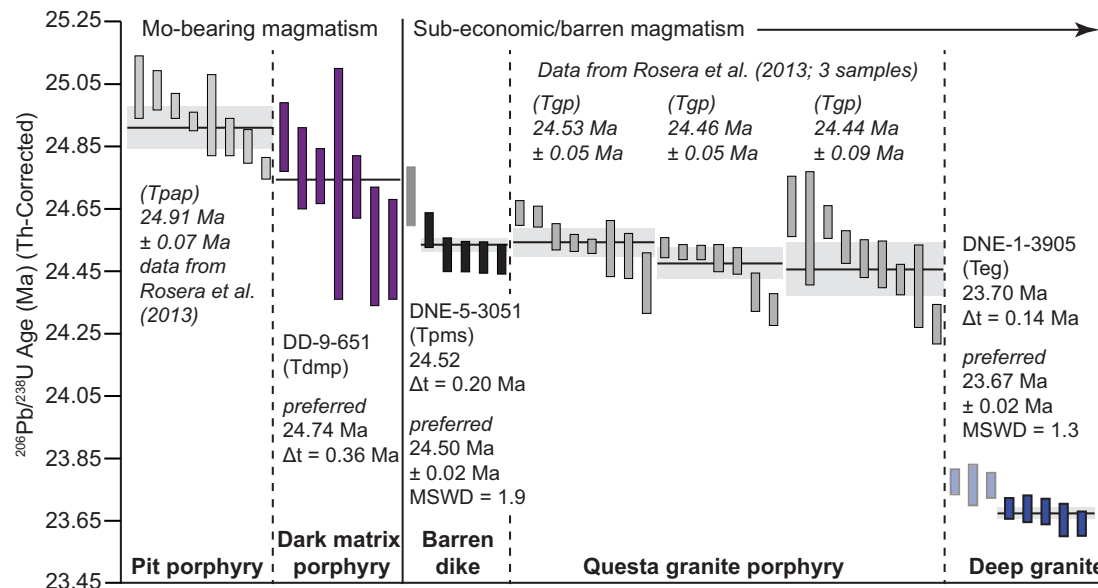


**Figure 12.**  $^{206}\text{Pb}/^{238}\text{U}$  ages for individual zircons for samples from the Latir magmatic center. Data are from this study, and relevant ages for the pit porphyry and Questa granite porphyry are from Rosera et al. (2013; gray data). Vertical bar height is  $2\sigma$  analytical uncertainties for individual analyses. As a result of the complicated spectrum and the poor analytical uncertainty of individual analyses, no uncertainty is estimated for the dark-matrix porphyry. Rather, we report the weighted-mean age (horizontal bar) and  $\Delta t$  between the ages of the oldest and youngest grains. For both the barren dike and the equigranular granite, we present the weighted mean and  $\Delta t$  for all grains and our preferred age—that is, the weighted mean and uncertainty for the youngest grains that overlap within uncertainty (horizontal bars and boxes, respectively). Grains not included in these weighted means are grayed out. See text for discussion.

from the dike overlap with those for zircons from the Questa granite porphyry (Rosera et al., 2013; Fig. 12). This suggests that the units either intruded in rapid succession or are part of the same system. In the latter case, the dike could represent an apophysis above the larger Questa granite porphyry. This is an intriguing possibility, because the Questa granite porphyry is capped nearly everywhere on the mine site by an ~0.05%  $\text{MoS}_2$  zone of mineralization—indicative of roofward volatile movement. If this is the case, the unmineralized nature of the dike requires that the Questa granite porphyry did not supply volatiles and metals upward as is commonly inferred in porphyry models.

The deep granite postdates mineralization and alteration at the central deposit and has a narrower age spectrum than any dated sample closely associated with hydrothermal activity (Fig. 12; 23.70 Ma;  $\Delta t = 0.14$  Ma). As for the barren dike, we prefer the interpretation that the older grains from this sample are antecrustic, and we accept the weighted mean and uncertainty of the youngest grains for the equigranular granite as the preferred age (23.67  $\pm$  0.02 Ma). Regardless of how the zircon age spectrum is interpreted in this sample, it intruded much later than the bulk of the overlying intrusions.

Previous molybdenite Re-Os geochronology showed that mineralization within the southwest ore zone occurred in at least three different pulses between ca. 24.8 and 24.5 Ma (Rosera et al., 2013). The nearby  $25.02 \pm 0.05$  Ma Cabresto Lake pluton (~3 km northeast of the mine; Figs. 1 and 2) is barren (Tappa et al., 2011) and has been interpreted to precede mineralization. The ages measured in this study, in conjunction with published ages, suggest that

magmatism and resulting mineralization within the central deposit must have occurred over ~500 ka at most (between 25.02 Ma [unmineralized Cabresto Lake zircon age] and 24.50 Ma [barren dike zircon age]). This is consistent with a growing body of evidence for episodic porphyry mineralization (e.g., Carten et al., 1988; Seedorff and Einaudi, 2004; Rosera et al., 2013; Chelle-Michou et al., 2015; Mercer et al., 2015b; Spencer et al., 2015; Rezeau et al., 2016).

### Defining Intrusive Units and Understanding Their Relationships

Modal mineralogy and textures of the intrusive units in this study indicate that a limited range of mineralogical variation and a broad range of textural variation exist at the Questa deposit, similar to what has been described for the well-characterized Henderson Mo deposit (Fig. 10; Table 3; Carten et al., 1988). Quartz, plagioclase, and K-feldspar are all common phenocryst phases in the intrusive rocks at Questa, but textures range from nearly aphyric to medium-grained porphyries. There is significant mineralogical overlap between some of the units identified in this study (Fig. 10; Table 3; note that some of the higher K-feldspar to plagioclase end members are potentially influenced by potassic alteration within ore zones). These data can be interpreted in two overlapping models: either the range of observed textures reflects variation in crystallization history of one or a few larger intrusions, or the observed units represent individual intrusive units.

### **Amphibole-Free Intrusions**

The mineralogical and textural overlap of many of the amphibole-free, generally quartz phenocryst-rich units could be interpreted as one or a few large magma bodies whose crystallization was influenced by loss of volatiles, quenching, and resurgence of deeper uncrystallized magma. This could explain some of the textural changes that are traceable across large portions of the mine. In particular, this model can explain the structural relationships of the central aplite, northeast porphyry, southwest porphyry, and Questa granite porphyry. Cooling of a large volume of magma results in a generally downward-moving crystallization front that interacts with magma and volatiles resupplied from below. Such a model predicts that the observed spatial correlation of textural changes and high-grade ore is the result of devolatilization near the downward-moving crystal + melt interface.

Field, alteration, and geochronologic evidence challenges the interpretation of the mineralogically similar units as a once large magma body, however. Crosscutting relationships consistently show an age progression of central aplite and/or northeast porphyry > pit porphyry > dark-matrix porphyry > southwest porphyry > Questa granite porphyry. The presence of clasts of central aplite within the dark-matrix porphyry in the southwest ore zone (Fig. 4B) requires that the central aplite was crystallized before the mineralogically distinctive dark-matrix porphyry intruded. The dark-matrix porphyry is cut by southwest and Questa granite porphyries in underground workings. This requires that the crystallized central aplite existed (at least in part) before these porphyries were intruded. Consequently, the quartz-phryic, amphibole-free southwest and Questa granite porphyries must have been dominantly intruded into preexisting plutons.

Examination of Figures 9 and 13 shows that the southwest porphyry is generally fine grained and only contains low- to moderate-temperature alteration mineral assemblages away from its contacts. It cuts coarser-grained, high-temperature altered central aplite (Fig. 13). If these units intruded all at once, it is difficult to reconcile the variation in degrees of alteration. Instead, the fine-grained groundmass and low-temperature alteration suggest new intrusions of southwest porphyry into already intensely altered wall rock. This is highlighted by sheets of the southwest porphyry in the vein zone orebody, where four downward-stacking intrusions of the same unit brecciated and mineralized the base of the solidified previous intrusion, amalgamating to an approximate thickness of 100 m (Figs. 7 and 8). It is unlikely that these sheets represent cooling units or resurgent units within one larger intrusion, because they can be traced to the west where they become vertically separated, cutting an older intrusive body composed mainly of central aplite (Fig. 8). High-temperature hydrothermal systems produced by magmatic fluid exsolution cooled and precipitated vein minerals multiple times throughout the assembly of the deposit, as evidenced by crosscutting veins and temperature reversals. This is likely due to the lack of persistent magmas within the Questa subsurface to add heat and additional fluids to the hydrothermal system.

Available geochronologic data support the field observations and the interpretation that the quartz-rich, amphibole-free Questa intrusions assembled

incrementally as many intrusions. Whereas there may be overlap at the high and low ends of zircon ages for sequential intrusions (as determined by cross-cutting relationships), there is no overlap for nonsequential intrusions (Fig. 12 and Rosera et al., 2013). Where there is overlap in ages from multiple samples of texturally similar rocks, we do interpret them to be parts of a single intrusion (e.g., the Questa granite porphyry; Fig. 12). Note, however, that there is no age overlap between the Questa granite porphyry and the younger deep granite (Fig. 12; Rosera et al., 2013).

### **Amphibole-Bearing Intrusions**

The unit that is most distinct mineralogically is the dark-matrix porphyry because it has sparse quartz phenocrysts, magnetite phenocrysts, and more abundant amphibole than other intrusions associated with the deposit (Fig. 10). The pit porphyry also has amphibole phenocrysts, and it seems plausible that these two map units could be parts of a single magma. In this scenario, field relations require that the dark-matrix porphyry intruded older, solidified parts of the magma chamber preserved as the pit porphyry. However, this requires that either (1) nearly all of the zircon analyzed from the pit porphyry by Rosera et al. (2013; Fig. 12) are antecryptic and that those zircons are absent from the dark-matrix porphyry, or (2) the dated zircons crystallized sequentially from an evolving magma—the pit porphyry from ca. 25.04–24.78 Ma (Rosera et al., 2013) and the dark-matrix porphyry from ca. 24.88–24.52 Ma (Table 5). If so, it is puzzling that there is so little overlap in the zircon populations and that the zircons do not show obvious temporal trends in Th/U (both have nearly identical Th/U from ~0.75–1.06) as documented in other studies (Samperton et al., 2015). Also, the range in crystallization ages for individual zircons from these intrusions (ca. 500 ka from 25.04 to 24.52 Ma; Fig. 12; Rosera et al., 2013) is too long for one large magma body in the upper crust (3–5 km paleodepth; Cline and Bodnar, 1994) that should have crystallized on the order of tens of ka, even with periodic magma replenishments (Cathles, 1981; Cathles et al., 1997). Consequently, we suggest that these two petrologically similar units are distinct intrusions. Overall, we concur with prior studies of the Questa deposit that suggest assembly was dominated by temporally discrete intrusions (Ross et al., 2002; Rosera et al., 2013).

### **Magmatic Assembly of the Central Deposit**

Mineralization in the Questa deposit occurred during the much longer magmatic history of the Latir magmatic center. The earliest efforts to understand the assembly of the center recognized three pluton-emplacement episodes that become younger and structurally deeper to the south, including (from north to south and oldest to youngest), resurgent, southern caldera margin, and southern plutons (Lipman et al., 1986). More recent detailed geochronology confirms the overall pattern of magmatism younging to the south (Tappa et

al., 2011; Zimmerer and McIntosh, 2012). Moreover, Tappa et al. (2011) suggest that the pattern is mimicked within the Rio Hondo pluton of the southern pluton group; that is, the data suggest that the pluton gets younger toward the structurally deeper exposed portions in the south. This pattern of downward stacking in the plutonic rocks is also documented in the Henderson Mo deposit (Seedorff and Einaudi, 2004).

The mineralized plutons of the Questa deposit all belong to the southern caldera margin group (Lipman et al., 1986). Crosscutting relationships and geochronology suggest that the plutons reflect the overall downward-younging sequence of the Latir magmatic system (Figs. 8, 14, and Animation 1). The central aplite is cut and underlain by the southwest porphyry, and both units are underlain by the younger Questa granite porphyry (Fig. 8). A similar vertical temporal sequence is present throughout the southwest ore zone, with the central aplite underlain by the pit porphyry intrusion, then the southwest porphyry, and finally, the Questa granite porphyry (Figs. 5–8 and 14, and Animation 1);

although, this structure is complicated by the pit porphyry cutting the central aplite east of the pit. In the deep northeast orebody, the 24.74 Ma dark-matrix porphyry is underlain by the ca. 24.5 Ma Questa granite porphyry, which is underlain by the 23.67 Ma equigranular granite (Fig. 6).

Our cross sections support the conclusions from earlier studies that the geometry of intrusions and mineralization at Questa were controlled by a (presently) north-dipping wall-rock anisotropy at the level of emplacement (Animation 1; Meyer, 1991; Ross et al., 2002). The orientation of intrusive roofs within the southwest ore zone has an average dip of 10° to north-northwest (Figs. 11B, 15). This matches the orientation of younger sedimentary and volcanic rocks north of Amalia, indicating that minor tilting postdates ca. 15 Ma (Lipman, 1983). Therefore, the intrusive rocks, their roofs, the mineralized zones, and the preexisting wall-rock anisotropy must also be tilted. Together with the relative chronology, this suggests that intrusions at Questa were originally roughly flat-lying sheets assembled in a broadly downward-stacking sequence.

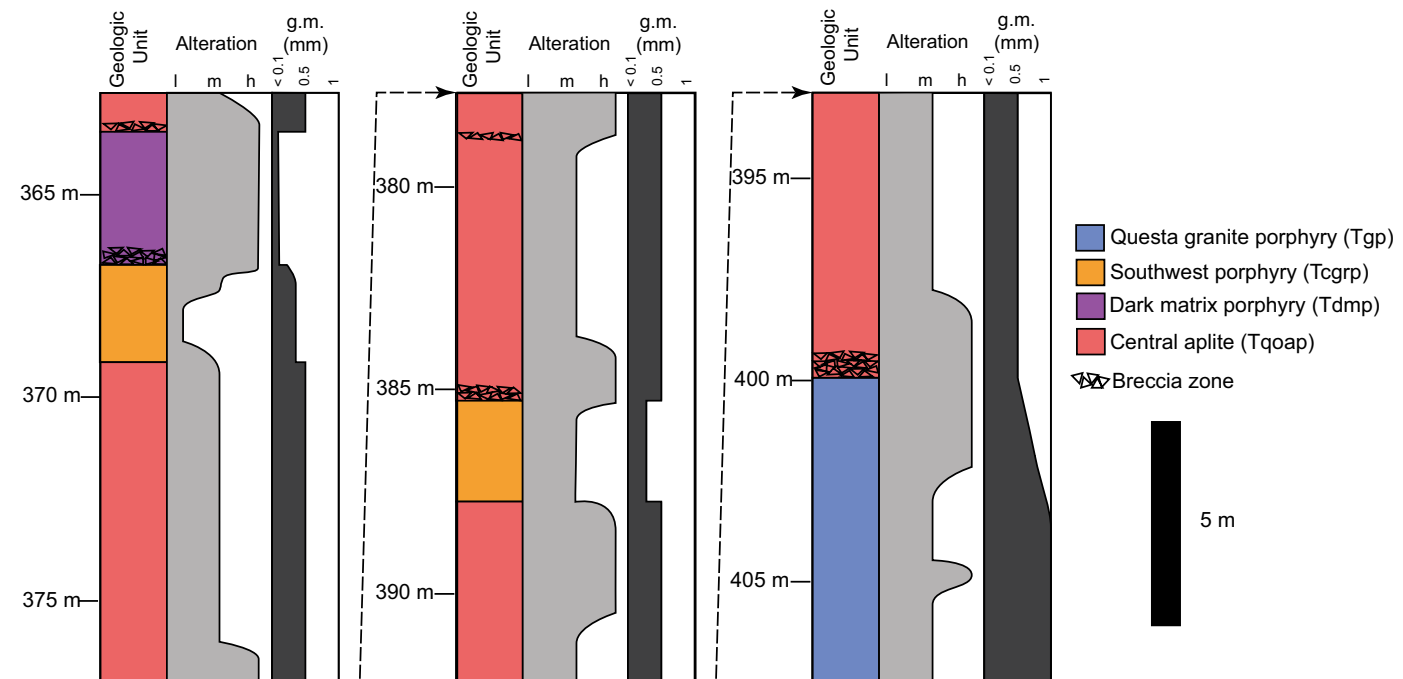


**Figure 13.** Simplified log of a single, continuous drill core from SWE-3 (an angled hole through the southwest extension orebody) showing the geologic units, maximum alteration temperature, and size of groundmass (g.m.). High-, medium-, and low-temperature alteration (h, m, l, respectively) are defined on the basis of the mineralogical classifications found in Table 2. High-temperature alteration zones are closely associated with the roofs of younger, crosscutting intrusions, as are zones of brecciation. Zones of high-temperature alteration commonly show moderate- and low-temperature alteration, with crosscutting relationships indicative of cooling. The roofs of both southwest porphyry and Questa granite porphyry often have quenched margin contacts, with groundmass becoming continuously coarser over ~1.5–7.5 m below the contact (e.g., Tcgrp ~367–368 m; Tgp ~400–405 m).

## Mineralization and Hydrothermal Alteration at Questa

### *The Central Deposit*

In all, at least five temporally discrete intrusive units at Questa are spatially associated with Mo ore within the central deposit and host high-temperature alteration at their roofs: the central aplite, northeast porphyry, pit porphyry, dark-matrix porphyry, and southwest porphyry (e.g., Figs. 5–8). On the basis of these observations and the discussion presented earlier, we conclude that bulk of the system intruded as relatively small batches of magma that crystallized completely, or nearly so, before the arrival of the next batch.

Ore shells at Questa typically project up-dip or are subparallel to the flat-lying sheets and roofs of the separate intrusions that we interpret as important for mineralization (e.g., Figs. 5–8). Moreover, ore shells are only present adjacent to, or directly within the upper portions of these intrusions. Structural measurements from the subsurface indicate that veins are oriented at a moderate angle ( $50^\circ$ ) relative to intrusive roof contacts (Fig. 11). This relationship is interpreted in other Climax-type deposits to reflect fluid exsolution directly from a proximal magma due to the relationship between high-angle veins and high-temperature alteration assemblages. At Questa, mineralized vein formation did not apparently involve significant meteoric fluids (Stein and Hannah, 1985; Carten et al., 1988; Seedorff and Einaudi, 2004). Therefore, we suggest that the central aplite, northeast porphyry, pit porphyry, dark-matrix porphyry, and southwest porphyry units were responsible for Mo mineralization at Questa, consistent with generation through hydrothermal fluid exsolution from upper-crustal intrusions as observed in other porphyry Mo systems (Carten et al., 1988).

### *The Spring Gulch and Log Cabin Deposits*

Work herein focused on the central deposit at Questa, but new observations about the Spring Gulch and log cabin deposits (Fig. 2) can also be made. Correlation of the Questa granite porphyry exposed at the surface in Sulphur Gulch with the Bear Canyon pluton was suggested by Rosera et al. (2013) because the two are the same age within uncertainty ( $24.44 \pm 0.086$  Ma;  $24.46 \pm 0.050$  Ma). This correlation is supported by published petrography (Johnson et al., 1989) and a structural interpretation by Meyer (1991), who suggested that the two exposures were a single plutonic sheet cut by high-angle normal faulting on both its eastern and western margins (Fig. 2). We suggest this sheet extends beyond surficial exposures and is correlative with the Questa granite porphyry underlying the central deposit. Because the Questa granite porphyry is not associated with economic mineralization in the Spring Gulch or central deposits, it seems unlikely that it could be associated with any at the log cabin deposit either. There, Mo mineralization is associated with several pre-Questa granite porphyry intrusive phases texturally similar to those in the central deposit and structurally above the Questa granite porphyry (Ratnaraj,

1967; though it is unclear if the mineralizing intrusions of the log cabin deposit directly correlate with the mineralizing intrusions of the central deposit).

### *Formation of the Hydrothermal Breccia (MHBX)*

The identification of discrete magmatic-hydrothermal events at Questa has important implications for the evolution of the ore-bearing MHBX (Fig. 4B) found in the southwest ore zone (Figs. 5–8; Ross et al., 2002). These breccia bodies, which are abundant at Questa but generally absent from other Climax-type deposits, are parallel to subparallel to the contact between intrusions and andesite wall rock (Fig. 8 and Animation 1). At Questa, the breccia bodies are important, but not exclusive, hosts for mineralization and are spatially associated with the central aplite. For example, the vein zone orebody has an ore shell similar to those in the Goat Hill, D-, and southwest orebodies, but it does not have a well-developed MHBX body (semi-stratified alteration; >30 m thick) or the presence of the central aplite (Figs. 7 and 8). Similarly, the deep northeast orebody lacks both an MHBX body and central aplite (Fig. 6). This suggests that the central aplite was essential for initiating brecciation.

We propose that the intrusion of the central aplite initiated brecciation and alteration along a low-angle preexisting anisotropy, and subsequent intrusions of ore-rich, dark-matrix porphyry, pit porphyry, and southwest porphyry mineralized and altered the MHBX bodies. The rarity of clasts in the MHBX with truncated Mo-bearing veins suggests that re-brecciation mainly cracked and mineralized the matrix. Each cycle of mineralization likely ended with the sealing of the matrix, which resulted in a pressure buildup, refracturing, and subsequent vein formation.

Molybdenite in the MHBX is both clotty (matrix hosted) and vein hosted. Individual breccia clasts in the MHBX that are encased within an alteration matrix including quartz-molybdenite veins suggest multiple molybdenite mineralization events were involved in creating these bodies. Molybdenite Re-Os geochronology established multiple episodes from  $24.76 \pm 0.03$ – $24.49 \pm 0.03$  Ma of both clotty and vein mineralization within MHBX (Rosera et al., 2013); these episodes are the result of multiple intrusions identified in this study. We hypothesize that the lack of correlation between semi-stratified MHBX alteration facies (Ross et al., 2002) and quartz-hosted fluid inclusion homogenization temperatures ( $620$ – $380$  °C; Rowe, 2012) is the result of overprinting of these cyclic mineralization events.

### *Intrusive Volumes at the Questa Mo Deposit and Implications for Climax-Type Models*

Using our interpretations of magmatic units and the cross sections generated for this study, we estimate that Mo-mineralizing magmas within the central deposit occupied  $\sim 0.62$  km $^3$  (Table 6). Although the 0.29 km $^3$  central aplite (nearly half of that total volume) contributed significantly to alteration

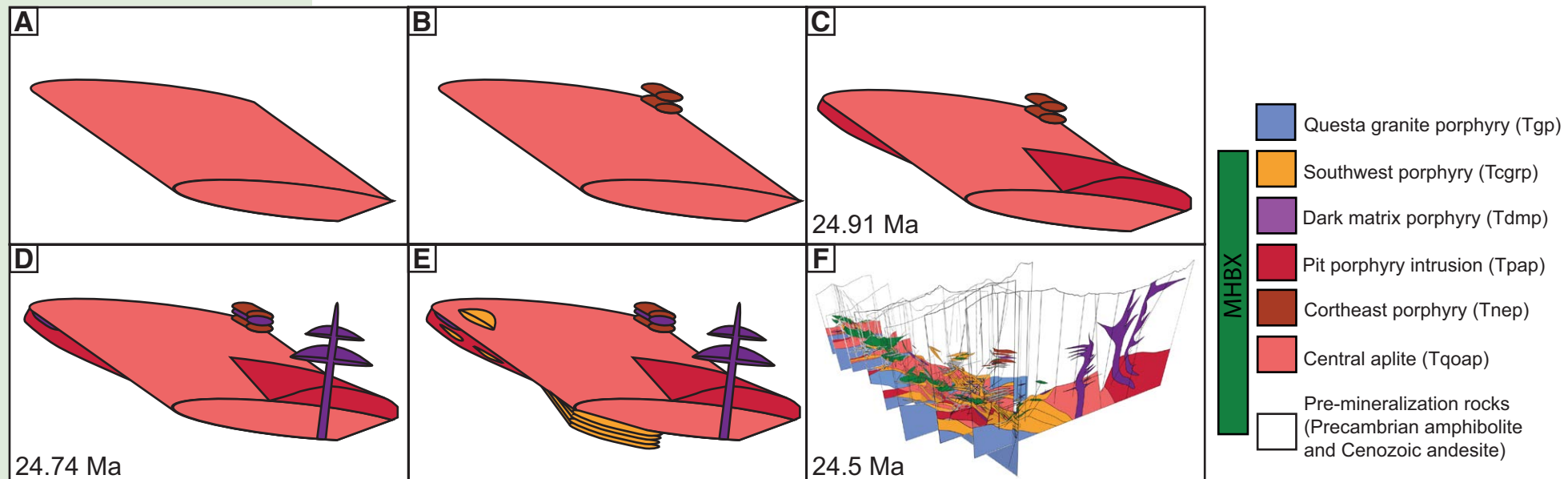


**Figure 14.** Schematic model of the emplacement sequence of intrusions associated with Mo mineralization at the Questa porphyry deposit. View is to the northwest. (A) Intrusion of the central aplite; (B) intrusion of the pit porphyry intrusion at 24.91 Ma (Rosera et al., 2013); (C) intrusion of sheets of the northeast porphyry; (D) intrusion of the dark-matrix porphyry at 24.74 Ma; (E) intrusion of the southwest porphyry; and (F) the deposit was underlain by the Questa granite porphyry at ca. 24.5 Ma (Rosera et al., 2013) and cut by the compositionally diverse post-mineralization suite beginning at 24.50 Ma. Magmatic-hydrothermal breccias are not included in this figure to emphasize the magmatic assembly of the deposit; however, they began formation during intrusion of the central aplite (A) and continued through intrusion of the southwest porphyry (E). See text for discussion.

and the generation of the MHBX bodies, there is no evidence that the central aplite directly deposited high-grade ore. Rather, throughout the southwest ore zone, an estimated total volume of  $0.07 \text{ km}^3$  comprises numerous dikes and sheets of the southwest porphyry that are responsible for high-grade ore. This is best demonstrated by the high-grade zones found outside of well-developed MHBX bodies within the vein zone orebody (Figs. 7 and 8).

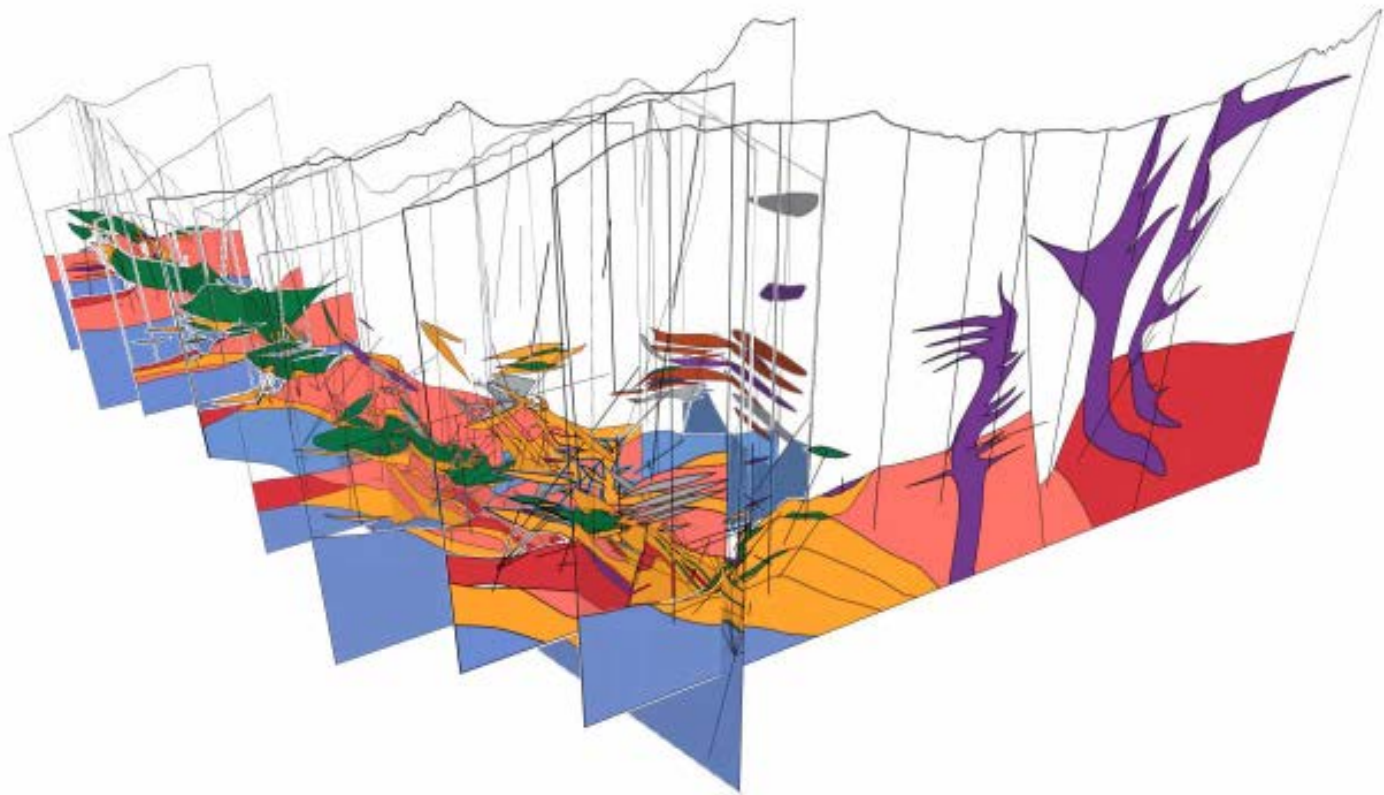
Within the northeast ore zone, the deep northeast orebody also highlights the role of small-volume intrusions in depositing significant ore (Fig. 6). The orebody is one of the volumetrically largest at Questa (at least  $9,375,000 \text{ m}^3$  above ore grade), and mineralization is associated with the northeast and dark-matrix porphyries. The northeast porphyry occurs as a series of five flat-lying intrusions separated by andesitic wall rock (Fig. 6). Only the bottom two sheets, which are intruded by heavily mineralized sheets of the dark-matrix porphyry, lack volcanic wall rock between them. Although these sheets may be connected out of section by a feeder, their geometry suggests that they are discrete sheeted intrusions. The northeast porphyry is cut by dark-matrix porphyry (Fig. 6), which is older than both the Questa granite porphyry (ca. 24.5 Ma) and the deep granite (ca. 23.7 Ma). These observations preclude the

possibility that any of the larger underlying intrusions could have supplied volatiles into the deep northeast orebody.

At Questa, high-grade ore is associated with small-volume intrusions. The larger-volume sheets in the southwest ore zone (e.g., central aplite and pit porphyry intrusion) are associated with Mo, below economic grade. The largest intrusion associated with the deposit, the Questa granite porphyry (estimated  $14.3 \text{ km}^3$ , minimum), postdates economic mineralization (compare the ore zones associated with the southwest and northeast porphyries and the lack of economic mineralization associated with the central aplite, pit porphyry, and Questa granite porphyry in Figs. 6 and 7). These observations imply that there was an inverse relationship between intrusion volume and the ability to generate high-grade mineralization at Questa.

We suggest that this observed negative correlation between magma volume and inferred mineralizing ability of intrusions at Questa indicates that focusing Mo-rich fluids through a long-lived magmatic conduit was probably not the dominant mechanism for mineralization. The observation that the high-grade deep northeast orebody was assembled by vertically discontinuous, small-volume sheets in conjunction with our interpretation that much of the

If reading the full-text version of this paper, please download article PDF to view Animation 1 in Adobe Acrobat or Adobe Reader. It is also available by visiting <http://doi.org/10.1130/GES01675.a1> or the full-text article on [www.gsapubs.org](http://www.gsapubs.org). Also available as Supplemental Item AE.



Animation 1. Rotating fence diagram of the southwest ore zone of the Questa Mo deposit, showing the three-dimensional relationships between Mo-mineralizing intrusions. From east to west, the N-S sections are: Supplemental Items C, G, and K (see text footnote 1) and Figure 6; Supplemental Items R, X, and BB (see text footnote 1) and Figure 7. The SW-NE section is Figure 8 and the E-W section in the deep northeast orebody is Supplemental Item DD (see text footnote 1). The fence diagram highlights: (1) the association of the orebodies with hydrothermal magmatic breccias and mineralizing intrusions; (2) the parallel to subparallel orientation of mineralizing intrusive sheets; (3) the relatively small volume of mineralizing intrusions relative to the non-mineralizing Questa granite porphyry; and (4) the generally downward-stacking structure of the intrusive system. If reading the full-text version of this paper, please download article PDF to view Animation 1 in Adobe Acrobat or Adobe Reader. It is also available by visiting <http://doi.org/10.1130/GES01675.a1> or the full-text article on [www.gsapubs.org](http://www.gsapubs.org). Also available as Supplemental Item AE.

TABLE 6. INTRUSIVE VOLUME ESTIMATES FOR THE QUESTA MOLYBDENUM DEPOSIT

Intrusive unit	Estimated volume (km <sup>3</sup> )
<b>Postmineralization intrusions</b>	
Questa granite porphyry	14.3*
<b>Molybdenum-mineralizing intrusions</b>	
Southwest porphyry	0.07
Dark-matrix porphyry	0.07
Pit porphyry intrusion	0.14
Northeast porphyry	0.04
Central aplite	0.29
<i>Note:</i> Intrusive volume estimates are based on cross sections (Figs. 5–8; Supplemental Items C–AD [see text footnote 1]) and surficial exposures.	
<i>*Minimum estimate due to faulting and deep exploration.</i>	

southwest ore zone formed above intrusions similar in size and composition to the older deep northeast orebody distinguish Questa from other porphyry mineralization systems. In particular, models that require rapid magmatic convection within a cylindrical conduit—such as that proposed by Shinohara et al. (1995) and recognized at Climax and Henderson Mo mines (White et al., 1981; Carten et al., 1988)—appear to be unable to explain the formation of (at least part of) the Questa deposit.

Thus, the Questa deposit may represent a structural end member of Mo-porphyry deposits. That is, assembly controlled by a low-angle anisotropy may be the reason that the Questa deposit does not have the stock and/or inverted-cup structure found at other Climax-type deposits (e.g., Dowsett et al., 1981; Carten et al., 1988), and this could have limited the ability of the magma system to establish a conduit that was optimal for mineralization. In this sense, the much higher grades and tonnages of Mo at the Climax and Henderson mines could represent an opposing end member characterized by intrusive shapes that were more optimized for mineralization. Alternatively, magmatic conduits that tie mineralizing intrusions to larger reservoirs at depth might only be active for rapidly advecting fluids upwards, rather than convecting volumes of magma.

Rapid movement of volatiles into the upper crust is hypothesized to have created a “contained explosion” in some porphyry Cu deposits, where diffusion modeling of vein envelope sizes suggests the entire magma system can degas in as few as 20–800 years (Cathles and Shannon, 2007). Our data support similar rapidity at Questa and suggest rapid devolatilization could have occurred numerous times through the lifespan of the magma system. Finally, we view these data as further evidence that ore deposition requires an alignment of numerous factors, including the magma source (Stein, 1985; Rosera et al., 2013; Mercer et al., 2015a), the degree and style of magma differentiation at depth (Audétat and Pettke, 2003; Audétat 2010; 2015), the role of mafic magmas (Keith et al., 1986; Mercer et al., 2015a), and the system’s ability to degas along conduits (Shinohara et al., 1995).

## CONCLUSIONS

Serial cross sections of the central deposit at Questa, New Mexico, paired with new geochronologic data, indicate the Questa Mo deposit was assembled from a series of small intrusions and has a complicated history of mineralization. This agrees with other well-studied Climax-type Mo deposits that are shown to form through episodic mineralization by multiple intrusive events. However, unlike other Climax-type deposits, we conclude that the mineralizing magmas at Questa were intruded as small-volume intrusions that amalgamated into a complicated, generally downward-stacking system, with geometries at least initially controlled by a preexisting fracture system associated with low-angle normal faults. Within the plutons at the Questa deposit, crosscutting alteration relationships and geochronology show that individual intrusions cooled quickly. The emplacement geometries of the intrusions controlled the expression of mineralization, causing Mo mineralization to be concentrated primarily within wall rock above their roofs. Economic Mo mineralization lasted for ~500 ka or less, beginning after ca. 25.02 Ma and ending before the emplacement of the barren dike and Questa granite porphyry at ca. 24.50 Ma. We interpret these data to suggest that any type of magmatic conduit for ascending volatiles at Questa would have been ephemeral, and numerous conduits were required to build the ore deposit rather than one long-lived magma column.

## ACKNOWLEDGMENTS

Funding was provided by National Science Foundation grant EAR 1220252 awarded to Coleman and the Geological Society of America, Sigma Xi Grants-in-Aid of Research, and the University of North Carolina Martin Fund. This project would not have been possible without the cooperation and breakfast burritos from Chevron Mining Inc., who provided access to mine property and drill core. Conversations with Bruce Walker were particularly helpful in developing this research. Thanks to Celestine Mercer, who provided a remarkably constructive review, Associate Editor Eric Christiansen, who challenged our ideas and sharpened our interpretations, and two anonymous reviewers who provided reviews that greatly improved this manuscript.

## REFERENCES CITED

- Allmendinger, R.W., Cardozo, N., and Fisher, D., 2011, Structural Geology Algorithms: Vectors and Tensors in Structural Geology: New York, Cambridge University Press, 304 p., <https://doi.org/10.1017/CBO9780511920202>.
- Annen, C., 2009, From plutons to magma chambers: Thermal constraints on the accumulation of eruptible silicic magma in the upper crust: *Earth and Planetary Science Letters*, v. 284, p. 409–416, <https://doi.org/10.1016/j.epsl.2009.05.006>.
- Audébat, A., 2010, Source and evolution of molybdenum in the porphyry Mo (-Nb) deposit at Cave Peak, Texas: *Journal of Petrology*, v. 51, p. 1739–1760, <https://doi.org/10.1093/petrology/egq037>.
- Audébat, A., 2015, Compositional evolution and formation conditions of magmas and fluids related to porphyry Mo mineralization at Climax, Colorado: *Journal of Petrology*, v. 56, p. 1519–1546, <https://doi.org/10.1093/petrology/egv044>.
- Audébat, A., and Pettke, T., 2003, The magmatic-hydrothermal evolution of two barren granites: a melt and fluid inclusion study of the Rito del Medio and Canada Pinabete Plutons in northern New Mexico (USA): *Geochimica et Cosmochimica Acta*, v. 67, p. 97–121, [https://doi.org/10.1016/S0016-7037\(02\)01049-9](https://doi.org/10.1016/S0016-7037(02)01049-9).
- Bloom, M.S., 1981, Chemistry of inclusion fluids: Stockwork molybdenum deposits from Questa, New Mexico, Hudson Bay Mountain, and Endako, British Columbia: *Economic Geology* and

- the *Bulletin of the Society of Economic Geologists*, v. 76, p. 1906–1920, <https://doi.org/10.2113/gsecongeo.76.7.1906>.
- Bowring, J.F., McLean, N.M., and Bowring, S.A., 2011, Engineering cyber infrastructure for U-Pb geochronology: Tripoli and U-Pb Redux: *Geochemistry, Geophysics, Geosystems*, v. 12, <https://doi.org/10.1029/2010GC003479>.
- Burnham, C.W., 1997, Magmas and hydrothermal fluids, in Barnes H.L., ed., *Geochemistry of Hydrothermal Ore Deposits* (third edition): New York, John Wiley and Sons, p. 63–123.
- Cardozo, N., and Allmendinger, R.W., 2013, Spherical projections with OSXStereonet: *Computers & Geosciences*, v. 51, p. 193–205, <https://doi.org/10.1016/j.cageo.2012.07.021>.
- Carten, R.B., Geraghty, E.P., Walker, B.M., and Shannon, J.R., 1988, Cyclic development of igneous features and their relationship to high-temperature hydrothermal features in the Henderson porphyry molybdenum deposit, Colorado: *Economic Geology and the Bulletin of the Society of Economic Geologists*, v. 83, p. 266–296, <https://doi.org/10.2113/gsecongeo.83.2.266>.
- Carten, R.B., White, W.H., and Stein, H.J., 1993, High-grade granite-related molybdenum systems: Classification and origin, in Kirkham, R.V., Sinclair, W.D., Thorpe, R.I., and Duke, J.M., eds., *Mineral Deposit Modeling*: Geological Association of Canada Special Paper 40, p. 521–544.
- Cathles, L.M., 1981, Fluid flow and genesis of hydrothermal ore deposits: *Economic Geology*, 75<sup>th</sup> Anniversary Volume, p. 424–457.
- Cathles, L.M., and Shannon, R., 2007, How potassium silicate alteration suggests the formation of porphyry ore deposits begins with the nearly explosive but barren expulsion of large volumes of magmatic water: *Earth and Planetary Science Letters*, v. 262, p. 92–108, <https://doi.org/10.1016/j.epsl.2007.07.029>.
- Cathles, L.M., Erendi, A.H.J., and Barrie, T., 1997, How long can a hydrothermal system be sustained by a single intrusive event?: *Economic Geology and the Bulletin of the Society of Economic Geologists*, v. 92, p. 766–771, <https://doi.org/10.2113/gsecongeo.92.7.766>.
- Chelle-Michou, C., Chiaradia, M., Selby, D., Ovtcharova, M., and Spikings, R.A., 2015, High resolution geochronology of the Corocchhuayco porphyry-skarn deposit, Peru: A rapid product of the Incaic orogeny: *Economic Geology and the Bulletin of the Society of Economic Geologists*, v. 110, p. 423–443, <https://doi.org/10.2113/econgeo.110.2.423>.
- Chiaradia, M., Schaltegger, U., and Spikings, R.A., 2014, Time scales of mineral systems—Advances in understanding over the past decade: *Society of Economic Geologists Special Publications*, v. 18, p. 37–58.
- Cline, J.S., and Bodnar, R.J., 1994, Direct evolution of a brine from a crystallizing silicic melt at Questa, New Mexico, molybdenum deposit: *Economic Geology and the Bulletin of the Society of Economic Geologists*, v. 89, p. 1780–1802, <https://doi.org/10.2113/gsecongeo.89.8.1780>.
- Dowsett, F.R., Ganster, M.W., Ranta, D.E., Baker, D.J., and Stein, H.J., 1981, Geology of the Mount Emmons Molybdenum deposit, Crested Butte, Colorado: *New Mexico Geological Society Guidebook*, 32nd Field Conference, Western Slope Colorado, p. 325–331.
- Gaynor, S.P., 2018, Modification of the crust: Mineralization and alteration in long-lived magmatic centers [Ph.D. dissertation]: University of North Carolina, Chapel Hill.
- Greber, N.D., Pettke, T., and Nagler, T.F., 2014, Magmatic-hydrothermal molybdenum isotope fractionation and its relevance to the igneous crustal signature: *Lithos*, v. 190–191, p. 104–110, <https://doi.org/10.1016/j.lithos.2013.11.006>.
- Hagstrum, J.T., and Johnson, C.M., 1986, A paleomagnetic and stable isotope study of the pluton at Rio Hondo near Questa, New Mexico: Implications for CRM related to hydrothermal alteration: *Earth and Planetary Science Letters*, v. 78, p. 296–314, [https://doi.org/10.1016/0012-821X\(86\)90069-5](https://doi.org/10.1016/0012-821X(86)90069-5).
- Hagstrum, J.T., and Lipman, P.W., 1986, Paleomagnetism of the structurally deformed Latir Volcanic Field, northern New Mexico: Relations to formation of the Questa Caldera and development of the Rio Grande Rift: *Journal of Geophysical Research*, v. 91, p. 7383–7402, <https://doi.org/10.1029/JB091iB07p07383>.
- Hoag, C.K., 2004, Molycorp Questa Mine: Subsidence Investigation: *Geologic Mapping and Cross Section Project*, unpublished report for Molycorp, Inc., 82 p.
- Johnson, C.M., Czamanske, G.K., and Lipman, P.W., 1989, Geochemistry of intrusive rocks associated with the Latir volcanic field, New Mexico, and contrasts between evolution of plutonic and volcanic rocks: *Contributions to Mineralogy and Petrology*, v. 103, p. 90–109, <https://doi.org/10.1007/BF00371367>.
- Keith, J.D., and Shanks, W.C., III, 1985, Chemical evolution and volatile fugacities of the Pine Grove porphyry molybdenum and ashflow tuff system, southwestern Utah, in Taylor, R.P., and Strong, D.F., eds., *Recent Advances in the Geology of Granite-Related Mineral Deposits*: Canadian Institute of Mining and Metallurgy Special Volume 39, p. 402–423.
- Keith, J.D., Shanks, W.C., III, Archibald, D.A., and Farrar, E., 1986, Volcanic and intrusive history of the Pine Grove porphyry molybdenum system, southwestern Utah: *Economic Geology* and the *Bulletin of the Society of Economic Geologists*, v. 81, p. 553–577, <https://doi.org/10.2113/gsecongeo.81.3.553>.
- Klemm, L., Pettke, T., and Heinrich, C.A., 2008, Fluid and source magma evolution of the Questa porphyry Mo deposit, New Mexico, USA: *Mineralium Deposita*, v. 43, p. 533–552, <https://doi.org/10.1007/s00126-008-0181-7>.
- Krogh, T.E., 1973, A low-contamination method for hydrothermal decomposition of zircon and extraction of U and Pb for isotopic age determinations: *Geochimica et Cosmochimica Acta*, v. 37, p. 485–494, [https://doi.org/10.1016/0016-7037\(73\)90213-5](https://doi.org/10.1016/0016-7037(73)90213-5).
- Lipman, P.W., 1983, The Miocene Questa caldera, northern New Mexico: Relation to batholith emplacement and associated molybdenum mineralization in Tucker, T.E., ed., *Proceedings of the Symposium on the Genesis of Rocky Mountain Ore Deposits: Changes with Time and Tectonics*: Denver Regional Exploration Geologists Society, p. 133–147.
- Lipman, P.W., and Reed, J.C., 1989, Geologic map of the Latir volcanic field and adjacent areas, northern New Mexico: U.S. Geological Survey Miscellaneous Investigations Series Map I-1907, scale 1:48,000.
- Lipman, P.W., Mehnert, H.H., and Naeser, C.M., 1986, Evolution of the Latir volcanic field, northern New Mexico, and its relation to the Rio Grande rift, as indicated by potassium-argon and fission track dating: *Journal of Geophysical Research*, v. 91, p. 6329–6345, <https://doi.org/10.1029/JB091iB06p06329>.
- Lowell, J.D., and Gilbert, J.M., 1970, Lateral and vertical alteration-mineralization zoning in porphyry ore deposits: *Economic Geology and the Bulletin of the Society of Economic Geologists*, v. 22, p. 893–896.
- Lowenstein, J., 1994, Dissolved volatile concentrations in an ore-forming magma: *Geology*, v. 22, p. 893–896, [https://doi.org/10.1130/0091-7613\(1994\)022<0893:DVCIAO>2.3.CO;2](https://doi.org/10.1130/0091-7613(1994)022<0893:DVCIAO>2.3.CO;2).
- Ludington, S., and Plumlee, G.S., 2009, Climax-type porphyry molybdenum deposits: U.S. Geological Survey Open-File Report 2009-1215, 16 p.
- Martineau, M.P., Heinemeyer, G.R., Craig, S.D., and McAndrews, K.P., 1977, Geological report, Questa Project: Questa, New Mexico, Questa Molybdenum Company, unpublished report, 161 p.
- Mattinson, J.M., 2005, Zircon U-Pb chemical abrasion ("CA-TIMS") method: Combined annealing and multi-step partial dissolution analysis for improved precision and accuracy of zircon ages: *Chemical Geology*, v. 220, p. 47–66, <https://doi.org/10.1016/j.chemgeo.2005.03.011>.
- McLean, N.M., Bowring, J.F., and Bowring, S.A., 2011, An algorithm for U-Pb isotope dilution data reduction and uncertainty propagation: *Geochemistry, Geophysics, Geosystems*, v. 12, <https://doi.org/10.1029/2010GC003479>.
- McLemore, V.T., and Mullen, K.E., 2004, Mineral resources in Taos County, New Mexico: New Mexico Geological Society Guidebook, 55th Field Conference, Geology of the Taos Region, p. 383–390.
- Mercer, C.M., Hofstra, A.H., Todorov, T.I., Roberge, J., Burgisser, A., Adams, D.T., and Cosca, M., 2015a, Pre-eruptive conditions of the Hideaway Park topaz rhyolite: Insights into metal source and evolution of magma parental to the Henderson porphyry molybdenum deposit, Colorado: *Journal of Petrology*, v. 56, p. 645–679, <https://doi.org/10.1093/petrology/egv010>.
- Mercer, C.M., Reed, R.H., and Mercer, C.M., 2015b, Time scales of porphyry Cu deposit formation: Insights from titanium diffusion in quartz: *Economic Geology and the Bulletin of the Society of Economic Geologists*, v. 110, p. 587–602, <https://doi.org/10.2113/econgeo.110.3.587>.
- Meyer, J., 1991, Volcanic, plutonic, tectonic, and hydrothermal history of the southern Questa caldera, New Mexico [Ph.D. thesis]: University of California at Santa Barbara, 384 p.
- Meyer, J., and Foland, K.A., 1991, Magmatic-tectonic interaction during early Rio Grande Rift extension at Questa, New Mexico: *Geological Society of America Bulletin*, v. 103, p. 993–1006, [https://doi.org/10.1130/0016-7606\(1991\)103<0993:MTIDER>2.3.CO;2](https://doi.org/10.1130/0016-7606(1991)103<0993:MTIDER>2.3.CO;2).
- Mundil, R., Ludwig, K.R., Metcalf, I., and Renne, P.R., 2004, Age and timing of the Permian mass extinctions: U/Pb dating of closed-system zircons: *Science*, v. 305, p. 1760–1763, <https://doi.org/10.1126/science.1101012>.
- Mutschler, F.E., Wright, E.G., Ludington, S., and Abbott, J.T., 1981, Granite Molybdenum systems: *Economic Geology and the Bulletin of the Society of Economic Geologists*, v. 76, p. 874–897, <https://doi.org/10.2113/gsecongeo.76.4.874>.
- Olsen, K.H., Baldridge, W.S., and Callender, J.F., 1987, Rio Grande rift: An overview: *Tectonophysics*, v. 143, p. 119–139, [https://doi.org/10.1016/0040-1951\(87\)90083-7](https://doi.org/10.1016/0040-1951(87)90083-7).
- Ovtcharova, M., Goudemand, N., Hammer, O., Gudoun, K., Cordey, F., Galfetti, T., Schaltegger, U., and Bucher, H., 2015, Developing a strategy for accurate definition of a geological boundary

- through radio-isotope and biochronological dating: The Early-Middle Triassic boundary (South China): *Earth-Science Reviews*, v. 146, p. 65–76, <https://doi.org/10.1016/j.earscirev.2015.03.006>.
- Parrish, R.P., 1987, An improved micro-capsule for zircon dissolution in U-Pb geochronology: *Chemical Geology*, v. 66, p. 99–192.
- Parrish, R.P., and Krogh, T.E., 1987, Synthesis and purification of  $^{205}\text{Pb}$  for U-Pb geochronology: *Chemical Geology*, v. 66, p. 103–110.
- Ratnaraj, D.H., 1967, Geology of the Log Cabin area, near Questa molybdenum mine, Taos County, New Mexico [M.S. thesis]: Tucson, University of Arizona, 104 p.
- Rezeau, H., Mortiz, R., Wotzlaw, J.F., Tayan, R., Melkonyan, R., Ulianov, A., Selby, D., d'Abzac, F.X., and Stern, R.A., 2016, Temporal and genetic link between incremental pluton assembly and pulsed porphyry Cu-Mo formation in accretionary orogens: *Geology*, v. 44, p. 627–630, <https://doi.org/10.1130/G38088.1>.
- Ricketts, J.W., Kelley, S.A., Karlstrom, K.E., Schmandt, B., Donahue, M.S., and van Wijk, J., 2016, Synchronous opening of the Rio Grande rift along its entire length at 25–10 Ma supported by apatite (U-Th)/He and fission-track thermochronology, and evaluation of possible driving mechanisms: *Geological Society of America Bulletin*, v. 128, p. 397–424, <https://doi.org/10.1130/B31223.1>.
- Rosera, J.M., Coleman, D.S., and Stein, H.J., 2013, Re-evaluating genetic models for porphyry Mo mineralization at Questa New Mexico: Implications for ore deposition following silicic ignimbrite eruption: *Geochemistry, Geophysics, Geosystems*, v. 14, p. 787–805, <https://doi.org/10.1002/ggge.20048>.
- Ross, P.S., Jebrak, M., and Walker, B.M., 2002, Discharge of hydrothermal fluids from a magma chamber and concomitant formation of a stratified breccia zone at the Questa porphyry molybdenum deposit, New Mexico: *Economic Geology* and the *Bulletin of the Society of Economic Geologists*, v. 97, p. 1679–1699, <https://doi.org/10.2113/gsecongeo.97.8.1679>.
- Rowe, A., 2012, Fluid evolution of the magmatic-hydrothermal breccia of the Goat Hill ore body, Questa Climax-type porphyry molybdenum system, New Mexico—A fluid inclusion study [Ph.D. thesis]: Socorro, New Mexico Institute of Mining and Technology, 269 p.
- Rudnick, R.L., and Gao, S.X., 2003, Composition of the continental crust: *Treatise on Geochemistry*, v. 3, p. 1–64.
- Samperton, K.M., Schoene, B., Cottle, J.M., Keller, C.B., Crowley, J.L., and Schmitz, M.D., 2015, Magma emplacement, differentiation and cooling in the middle crust: Integrated zircon geochronological-geochemical constraints from the Bergell Intrusion, Central Alps: *Chemical Geology*, v. 417, p. 322–340, <https://doi.org/10.1016/j.chemgeo.2015.10.024>.
- Schaltegger, U., and Davies, J.H.F.L., 2017, Petrochronology of zircon and baddeleyite in igneous rocks: Reconstructing magmatic processes at high temporal resolution: *Reviews in Mineralogy and Geochemistry*, v. 83, p. 297–328, <https://doi.org/10.2138/rmg.2017.83.10>.
- Schaltegger, U., Brack, P., Ovtcharova, M., Peytcheva, I., Schoene, B., Stracke, A., Marocchi, M., and Bargossi, G.M., 2009, Zircon and titanite recording 1.5 million years of magma accretion, crystallization and initial cooling in a composite pluton (southern Adamello batholith, northern Italy): *Earth and Planetary Science Letters*, v. 286, p. 208–218, <https://doi.org/10.1016/j.epsl.2009.06.028>.
- Schoene, B., Samperton, K.M., Eddy, M., Keller, G., Adatte, T., Bowring, S.A., Khadri, S.R., and Gertsch, B., 2015, U-Pb geochronology of the Deccan Traps and relation to the end-Cretaceous mass extinction: *Science*, v. 347, p. 182–184, <https://doi.org/10.1126/science.aaa0118>.
- Seedorff, E., and Einaudi, M.T., 2004, Henderson porphyry molybdenum system, Colorado: I. Sequence and abundance of hydrothermal mineral assemblages, flow paths of evolving fluids, and evolutionary style: *Economic Geology* and the *Bulletin of the Society of Economic Geologists*, v. 99, p. 3–37.
- Seo, J.H., 2014, Hydrothermal sulfur geochemistry on molybdenite deposition of the Questa Mo-deposit, New Mexico, USA: *Geosciences Journal*, v. 18, p. 419–425, <https://doi.org/10.1007/s12303-014-0040-8>.
- Shannon, J.R., Walker, B.M., Carten, R.B., and Geraghty, E.P., 1982, Unidirectional solidification textures and their significance in determining relative age of intrusions at the Henderson Mine, Colorado: *Geology*, v. 10, p. 293–297, [https://doi.org/10.1130/0091-7613\(1982\)10<293:USTATS>2.0.CO;2](https://doi.org/10.1130/0091-7613(1982)10<293:USTATS>2.0.CO;2).
- Shinohara, H., Kazahaya, K., and Lowenstern, J.B., 1995, Volatile transport in a convecting magma column: Implications for porphyry Mo mineralization: *Geology*, v. 23, p. 1091–1094, [https://doi.org/10.1130/0091-7613\(1995\)023<1091:VTIACM-2.3.CO;2](https://doi.org/10.1130/0091-7613(1995)023<1091:VTIACM-2.3.CO;2).
- SketchUp, 2016, <http://www.sketchup.com> (accessed 10 August 2016).
- Snyder, G.R., 1984, Paleomagnetism of the Questa mine area, Taos County, New Mexico [M.S. thesis]: Golden, Colorado School of Mines, 111 p.
- Spencer, E.T., Wilkinson, J.J., Creaser, R.A., and Seguel, J., 2015, The distribution and timing of molybdenite mineralization at the El Teniente Cu-Mo porphyry deposit, Chile: *Economic Geology* and the *Bulletin of the Society of Economic Geologists*, v. 110, p. 387–421, <https://doi.org/10.2113/econgeo.110.2.387>.
- Steiger, R.H., and Jäger, E., 1977, Subcommission of geochronology: Convention on the use of decay constants in geo- and cosmo-chemistry: *Earth and Planetary Science Letters*, v. 36, no. 3, p. 359–362, [https://doi.org/10.1016/0012-821X\(77\)90060-7](https://doi.org/10.1016/0012-821X(77)90060-7).
- Stein, H.J., 1985, A Lead, Strontium, and Sulfur Isotope Study of the Laramide-Tertiary Intrusions and Mineralization in the Colorado Mineral Belt with Emphasis on Climax-type Porphyry Molybdenum Systems plus a Summary of Other Newly Acquired Isotopic and Rare Earth Element Data [Ph.D. thesis]: University of North Carolina at Chapel Hill, 493 p.
- Stein, H.J., and Hannah, J., 1985, Movement and origin of ore fluids in Climax-type systems: *Geology*, v. 13, p. 469–474, [https://doi.org/10.1130/0091-7613\(1985\)13<469:MAOOOF>2.0.CO;2](https://doi.org/10.1130/0091-7613(1985)13<469:MAOOOF>2.0.CO;2).
- Tappa, M.J., Coleman, D.S., Mills, R.D., and Samperton, K.M., 2011, The plutonic record of a silicic ignimbrite from the Latir volcanic field, New Mexico: *Geochemistry, Geophysics, Geosystems*, v. 10, <https://doi.org/10.1029/2011GC003700>.
- Taylor, S.R., and McLennan, S.M., 1995, The geochemical evolution of the continental crust: *Reviews of Geophysics*, v. 33, p. 241–265, <https://doi.org/10.1029/95RG00262>.
- von Quadt, A., Erni, M., Martinek, K., Moll, M., Peytcheva, I., and Heinrich, C.A., 2011, Zircon crystallization and the lifetimes of ore-forming magmatic-hydrothermal systems: *Geology*, v. 39, p. 731–734, <https://doi.org/10.1130/G31966.1>.
- Wallace, S.R., Muncaster, N.K., Jonson, D.C., MacKenzie, W.B., Bookstrom, A.A., and Surface, V.E., 1968, Multiple intrusion and mineralization at Climax, Colorado, in Ridge, J.D., ed., *Ore Deposits of the United States, 1933–1967*: New York, American Institute of Mining Metallurgy and Petroleum Engineers, p. 605–640.
- White, W.H., Bookstrom, A.A., Kamilli, R.J., Ganster, M.W., Smith, R.P., Ranta, D.E., and Steininger, R.C., 1981, Character and origin of Climax-type molybdenum deposits: *Economic Geology* 75th Anniversary Volume, p. 270–316.
- Wotzlaw, J.F., Schaltegger, U., Frick, D.A., Dungan, M.A., Gerdes, A., and Gunther, D., 2013, Tracking the evolution of large-volume silicic magma reservoirs from assembly to supereruption: *Geology*, v. 41, p. 867–870, <https://doi.org/10.1130/G34366.1>.
- Zimmerer, M.J., and McIntosh, W.C., 2012, The geochronology of volcanic and plutonic rocks at the Questa caldera: Constraints on the origin of caldera-related silicic magmas: *Geological Society of America Bulletin*, v. 124, p. 1394–1408, <https://doi.org/10.1130/B30544.1>.